

# Statistical bias correction for creating coherent total ozone record from OMI and OMPS observations



Kaixu Bai<sup>a,b</sup>, Ni-Bin Chang<sup>b,\*</sup>, Huijia Yu<sup>c</sup>, Wei Gao<sup>a,d</sup>

<sup>a</sup> Key Laboratory of Geographic Information Science, Ministry of Education, East China Normal University, Shanghai 200241, China

<sup>b</sup> Department of Civil, Environmental, and Construction Engineering, University of Central Florida, Orlando, FL 32816, USA

<sup>c</sup> Trinity College of Arts and Sciences, Duke University, Durham, NC 27708, USA

<sup>d</sup> USDA UV-B Monitoring and Research Program, Natural Resource Ecology Laboratory, and Department of Ecosystem Science and Sustainability, Colorado State University, Fort Collins, CO 80523, USA

## ARTICLE INFO

### Article history:

Received 16 July 2015

Received in revised form 16 March 2016

Accepted 15 May 2016

Available online xxxx

### Keywords:

Total column ozone

Bias correction

Data merging

Remote sensing

## ABSTRACT

A long-term coherent total column ozone (TCO) record is essential to ozone layer variability assessment, especially the detection of early signs of ozone recovery after years of depletion. Because of differences in satellite platforms and instruments design, calibration, and retrieval algorithms, however, significant cross-mission biases are observed between multiple sensor TCO observations in the common time–space domain. To attain a coherent TCO record, observed cross-mission biases should be accurately addressed prior to the data-merging scheme. In this study, a modified statistical bias correction method was proposed based on the quantile–quantile adjustment to remove apparent cross-mission TCO biases between the Ozone Monitoring Instrument (OMI) and Ozone Mapping and Profiler Suite (OMPS). To evaluate the effectiveness of this modified algorithm, the overall inconsistency (OI), a unique time-series similarity measure, was proposed to quantify the improvements of consistency (or similarity) between cross-mission TCO time series data before and after bias correction. Common observations during the overlapped time period of 2012–2015 were used to characterize the systematic bias between OMPS and OMI through the modified bias correction method. TCO observations from OMI during 2004–2015 were then projected to the OMPS level by removing associated cross-mission biases. This modified bias correction scheme significantly improved the overall consistency, with an average improvement of 90% during the overlapped time period at the global scale. In addition to the evaluation of consistency improvements before and after bias correction, impacts of cross-mission biases on long-term trend estimations were also investigated. Comparisons of derived trends from the merged TCO time series before and after bias correction across 38 ground-based stations indicate that cross-mission biases not only affect magnitudes of estimated trends, but also result in different phases of trends. Further comparisons of estimated seasonal TCO trends before and after bias correction at the global scale suggest that trends derived from the bias-corrected time series are more accurate than those without bias correction. Overall, the bias correction scheme developed in this study is essential for preparing an accurate long-term TCO record representative of trend analysis to support future assessment of ozone recovery at the global scale.

© 2016 Elsevier Inc. All rights reserved.

## 1. Introduction

Ozone is an important atmospheric component that plays a key role in atmospheric chemical and radiation processes, despite its smaller concentration compared to the well-mixed carbon dioxide in the atmosphere (Jöckel et al., 2006; McPeters, Bhartia, Haffner, Labow, & Flynn, 2013). Broadly, atmospheric ozone can be divided into two portions depending on its location in the atmosphere: stratospheric ozone in the Earth's upper atmosphere and tropospheric ozone in the lower atmosphere. Unlike ozone in the troposphere, which adversely impacts

human health, natural vegetation growth, and crop yield, stratospheric ozone protects life on Earth from the sun's harmful ultraviolet (UV) light by absorbing the high frequency radiation through a photochemical process. This process modifies the chemistry of the stratosphere and produces heat that in turn changes atmospheric dynamics (McPeters et al., 2013).

Compared to the “bad ozone” at the Earth's surface, “good ozone” in the stratosphere draws more scientific attention because of the dramatic ozone depletion over Antarctica and its profound climatic effects on the global environment since the late 1970s. As a result of the abundant release of anthropogenic chlorofluorocarbons into the atmosphere, an expanding Antarctic ozone hole has been observed during each austral spring in the past decades. Scientific investigations indicate that the

\* Corresponding author.

depleted Antarctic ozone layer has played a critical role in the Southern Hemisphere (SH) climate changes, and that these effects are not confined just to the vicinity of Antarctica but extend over much of the SH, even reaching the tropics (e.g., Reason, 2005; Son, Tandon, Polvani, & Waugh, 2009; Thompson et al., 2011; Kang, Polvani, Fyfe, & Sigmond, 2011; Ding, Steig, Battisti, & Küttel, 2011; Feldstein, 2011; Fyfe, Gillett, & Marshall, 2012; Gillett, Fyfe, & Parker, 2013; Gonzalez, Polvani, Seager, & Correa, 2013; Manatsa, Morioka, Behera, Yamagata, & Matarira, 2013). Owing to the implementation of the Montreal Protocol and its amendments since 1989, emissions of ozone depleting substances into the atmosphere have been significantly reduced. Subsequently, ozone layer depletion has decelerated and has begun to recover since the mid-1990s (WMO, 2003). Modeling experiments indicate that the ozone layer would recover to its 1980s conditions by the 2050s, which in turn may result in significant climatic changes (e.g. Arblaster, Meehl, & Karoly, 2011; Perlwitz, 2011; Perlwitz, Pawson, Fogt, Nielsen, & Neff, 2008; Barnes, Barnes, & Polvani, 2014; Previdi & Polvani, 2014).

To better predict future climate, investigations of mechanisms linking the regional climate changes to the observed ozone variability are needed, and therefore accurate long-term total column ozone (TCO) records are critical. These records are also essential to better understand earth system processes, to assess TCO variability and long-term trends, and to provide inputs to modeling efforts of Earth systems. Since the late 1970s, satellite-based TCO observations with high temporal resolution (e.g., daily) at the global scale have been available. Different satellite instruments and platforms have provided TCO observations since the 1970s (Fig. 1). These cross-mission sensors provide continuous TCO observations for long-term variability assessment. Because of differences in platforms and instruments design, calibration processes, center wavelengths, and retrieval algorithms, however, apparent cross-mission biases are observed between associated TCO observations. As reported by Kuttippurath et al. (2013), however, an ozone recovery rate of 1 to 2.6 Dobson Units (DU) per year was observed during 2000–2010 over Antarctica, which in turn suggests that even small drifts between TCO time series could result in apparent changes

in ozone layer recovery speed. To create a consistent TCO record for the assessment of the long-term ozone variability, particularly the early signs of ozone recovery, cross-mission biases should be removed prior to the merging scheme. Generally, an advanced approach is to reprocess all the original radiometric datasets by applying different calibration corrections to each instrumental observation to guarantee that data from different instruments are consistent prior to the retrieval process through a same algorithm (McPeters et al., 2013). This approach is accurate because radiance calibration errors propagate nonlinearly, producing latitudinal and seasonal dependent errors in the retrieved ozone data (McPeters et al., 2013). One representative product using this approach is the Version 8.6 Solar Backscatter Ultraviolet (SBUV) Merged Ozone Data Set (MOD), which provides the longest available satellite-based time series TCO profile from a single instrument type (i.e., SBUV-type) (Frith et al., 2014; MCPeters et al., 2013). A similar product was also created from European satellite sensor observations (e.g., Lerot et al., 2014). Although this approach is accurate, establishing a consistent calibration for different instruments requires efforts that can only be achieved by working with the original instrument teams. Moreover, the current Version 8.6 SBUV MOD is a zonal monthly mean gridded product with a spatial resolution of 5° globally, and both spatial and temporal resolutions are too coarse for regional analysis such as ozone-hole monitoring. In addition to the aforementioned reprocessing approach, data assimilation is another possible method capable of creating a long-term TCO record by incorporating TCO observations from satellite and ground-based instruments simultaneously. TCO records generated from these methods are always referred to as multi-sensor reanalysis ozone (e.g., Dragani, 2011; Van Der, J., Allaart, & Eskes, 2010, 2015).

In addition to the aforementioned complex approaches, statistical bias correction methods could be alternatives to removing cross-mission sensors biases. Most widely used statistical bias correction methods include simple approaches such as the delta-change and linear scaling (e.g. Vila, de Goncalves, Toll, & Rozante, 2009; Teutschbein & Seibert, 2012), and higher-skill methods such as the nonlinear regression (e.g. Teutschbein & Seibert, 2012; Bordoy & Burlando, 2013), Kalman

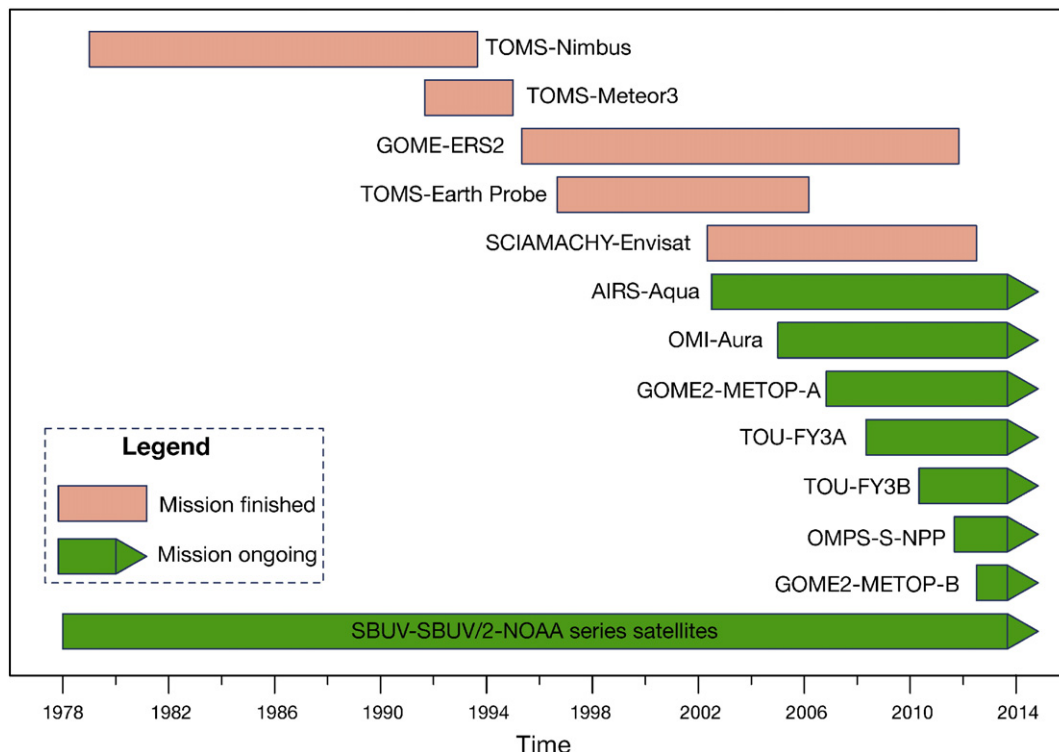


Fig. 1. Satellite instruments and platforms providing total ozone measurements since the 1970s.

**Table 1**  
Characteristics of TCO observations from OMPS and OMI used in this study.

Product	Sensor	Satellite	Spatial resolution	Temporal resolution	Algorithm	Time span	Data provider
EDR_TO3_L3	OMPS	S-NPP	1°	Daily	SBUV V8.6	2012.1–2015.3	OMPS science team <sup>a</sup>
OMTO3d	OMI	Aura	1°	Daily	TOMS V8.5	2004.10–2015.3	OMI science team <sup>b</sup>

<sup>a</sup> NASA's Goddard Space Flight Center/OMPS science team. <https://ozoneaq.gsfc.nasa.gov>.

<sup>b</sup> NASA's Goddard Space Flight Center/OMI science team. [http://disc.gsfc.nasa.gov/datacollection/OMTO3d\\_V003.html](http://disc.gsfc.nasa.gov/datacollection/OMTO3d_V003.html).

filtering (e.g. Delle Monache, Nipen, Deng, Zhou, & Stull, 2006; Sicardi et al., 2012), and distribution mapping (e.g., Li, Sheffield, & Wood, 2010; Piani, Weedon, Best, Gomes, Viterbo et al., 2010; Piani, Haerter & Coppola, 2010; Haerter, Hagemann, Moseley, & Piani, 2011; Hagemann et al., 2011; Ahmed et al., 2013; Argüeso, Evans, & Fita, 2013; Bai, Chang, & Chen, 2016). These methods have been applied to correct climate modeling biases to better predict future scenarios. Nevertheless, some limitations associated with various methods persist. For example, simple methods such as delta-change and linear scaling only address the common biases between observations and modeling outputs, meaning these methods are incapable of handling nonlinear biases with dependencies; however, results from nonlinear methods such as aforementioned neural networks are prone to influence by the training inputs. If the training inputs do not cover enough samples, the outputs could be biased. Kalman filtering, widely used in removing modeling biases in forecasting processes, cannot readily address biases in discrete time series because these biases are always estimated from previous observations and forecasts in a cascaded way. In general, higher-skill bias correction methods, such as distribution mapping, perform better than simple methods due to their adaptive adjustment schemes and thus can be widely adopted (Lafon, Dadson, Buys, & Prudhomme, 2013; Teutschbein & Seibert, 2013).

Common observations between cross-mission sensors in the overlapped time period allow quantification of discrepancies between sensors through inter-instruments comparisons (Barnes & Hu, 2015). The most straightforward method is to build relationships with matchups between cross-mission sensors observations through either linear or nonlinear regressions. For instance, with stacked neural networks, temporal and spatial drifts between TCO from three European satellite sensors were characterized and used sequentially to adjust satellite

observations from different sensors to create a global homogeneous long-term TCO record (Loyola & Coldewey-Egbers, 2012). In addition, cross-mission biases can also be removed by calibrating satellite observations with collocated ground-based measurements. For example, to improve the consistency of ocean color data derived from Sea-viewing Wide Field-of-view Sensor (SeaWiFS) and Moderate Resolution Imaging Spectroradiometer (MODIS), both sensors observations were mapped onto the in situ measurements for bias correction and then merged (Gregg & Casey, 2010), a process referred to as vicarious calibration. Similar bias correction schemes through vicarious calibration can also be found in other studies (e.g., D'Alimonte, Zibordi, & Mélin, 2008; Hoyer, Le Borgne, & Eastwood, 2013); however, limitations of these bias correction schemes are also obvious. First, if cross-mission sensor biases are spatially heterogeneous, in situ observations alone are not capable of removing all the cross-mission biases effectively on an operational basis because abundant in situ measurements are lacking. Second, addressing biases with latitudinal and seasonal dependent features is difficult. Some of the higher-skill bias correction methods could respond to these needs.

In this study, to demonstrate the necessity and the effectiveness of the proposed algorithm, TCO observations from the Ozone Mapping and Profiler Suite (OMPS) on board the Suomi National Polar-orbiting Partnership (S-NPP) satellite and Ozone Monitoring Instrument (OMI) on board the Aura satellite were applied. The reason for selecting TCO data from OMPS and OMI is that their data are generally compatible with each other in the common time-space domain and considered to be synergistic over the observational period. Even with these two highly accurate datasets, however, cross-mission biases are observed between them, possibly resulting in inaccurate rate of ozone recovery estimation. The objectives of this study were thus to: 1) develop a modified

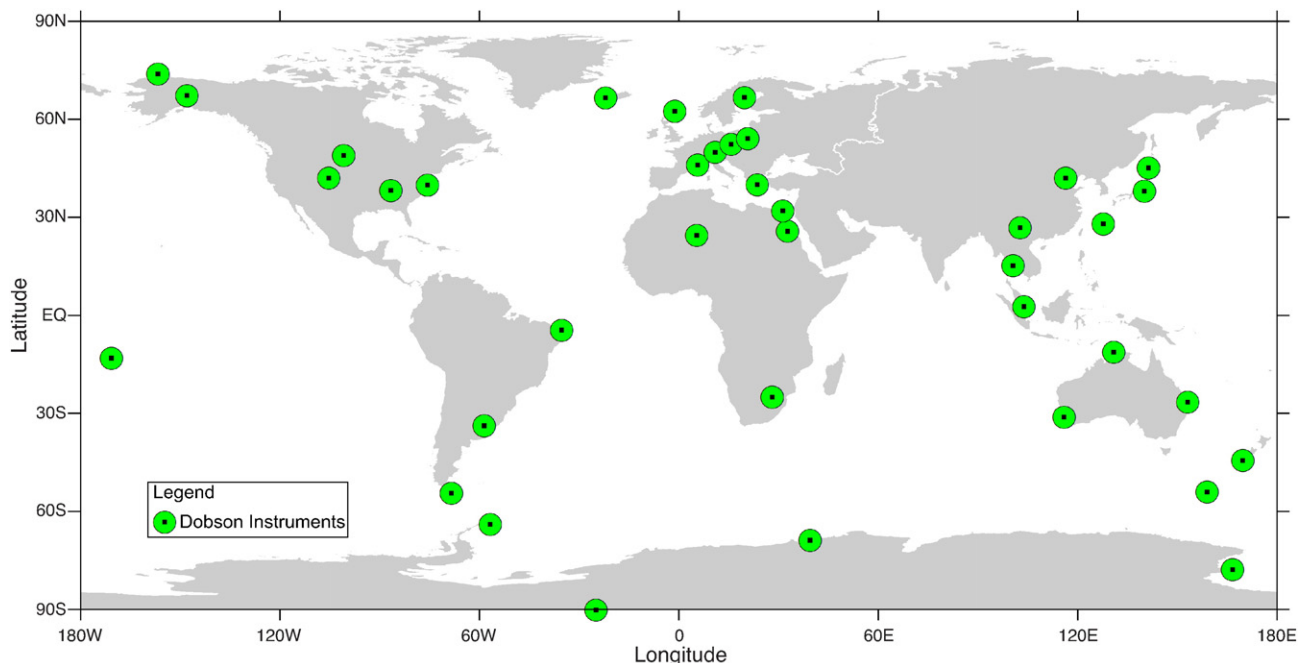


**Fig. 2.** Spatial distribution of 38 ground-based Dobson instruments providing TCO measurements used as ground-based references in this study.

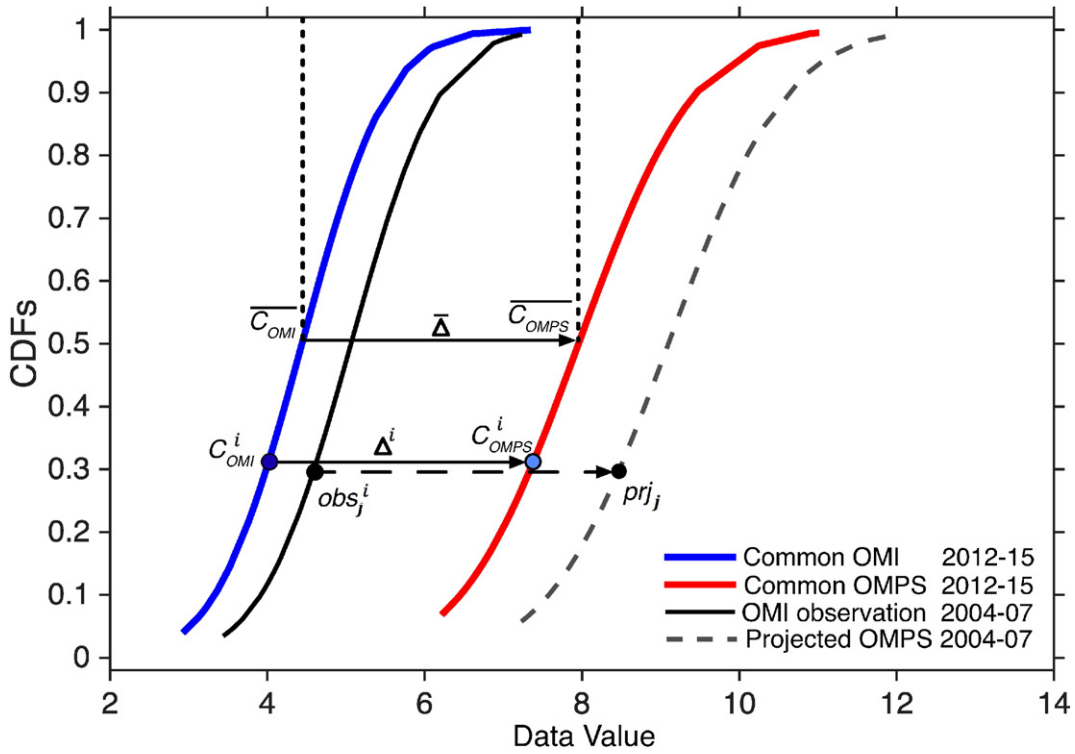


**Fig. 3.** Schematic plot of the original Q-Q adjustment method for removing cross-mission TCO biases between OMPS and OMI. Note that the raw observations (OMI observation: thick black line) have a time scale (3 years: 2004–2007) the same as that (3 years: 2012–2015) of two control observations (common observations of OMI and OMPS: blue and red lines), meaning that calibrating a length of 3 years OMI observations (i.e., 2004–2007) to OMPS level requires the same length of control observations during the overlapping time period between OMI and OMPS (i.e., 2012–2015). The projected OMPS denotes the anticipated data at the OMPS level that should be corrected from the OMI observations. (For interpretation of the references to color in this figure legend, the reader is referred to the web version of this article.)

statistical bias correction method that can be applied to remove apparent cross-mission TCO biases between OMPS and OMI; 2) cast a unique

time series similarity measure, the overall inconsistency (OI), to evaluate the performance of this modified statistical bias correction method

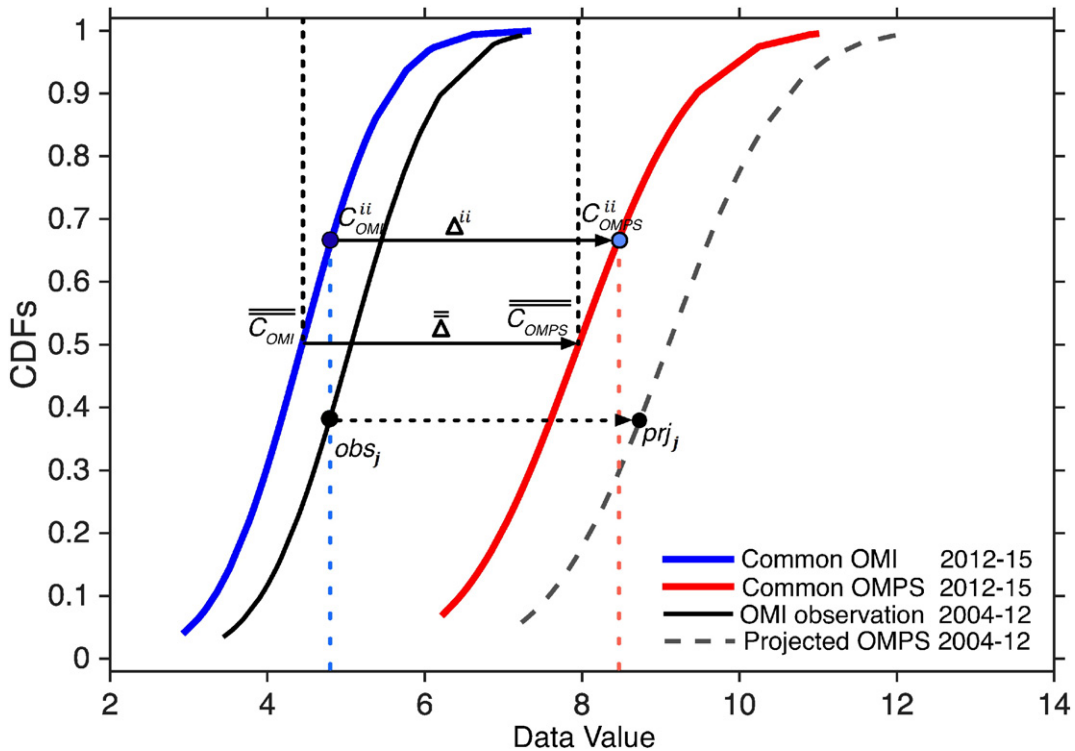


**Fig. 4.** Distribution mapping for the modified method. Note that the raw observations (thick black line) have a time scale (8 years: 2004–2012) different from that (3 years: 2012–2015) of two control observations (blue and red lines). (For interpretation of the references to color in this figure legend, the reader is referred to the web version of this article.)

to address significant latitudinal and seasonal dependent biases and quantify the consistency improvements before and after bias correction; and 3) evaluate the impacts of cross-mission biases on trend analysis. Two science questions were proposed for this study: 1) How can inherent constraining and enhancing factors for data merging of common observation within the overlapped time period be extracted and related to actual changes in final data merging processes? 2) To what extent can the cross-mission biases affect the accuracy of estimated TCO trends in long-term assessment of ozone recovery at the global scale?

## 2. Satellite and ground-based TCO data

In this study, Level-3 TCO observations collected from OMPS and OMI (characteristics in Table 1) were used collectively to generate a merged long-term, consistent TCO record. Ground-based TCO measurements collected from the World Ozone and Ultraviolet radiation Data Centre (WOUDC) were also used as ground references to assess the consistency improvement of the merged TCO record before and after bias correction.

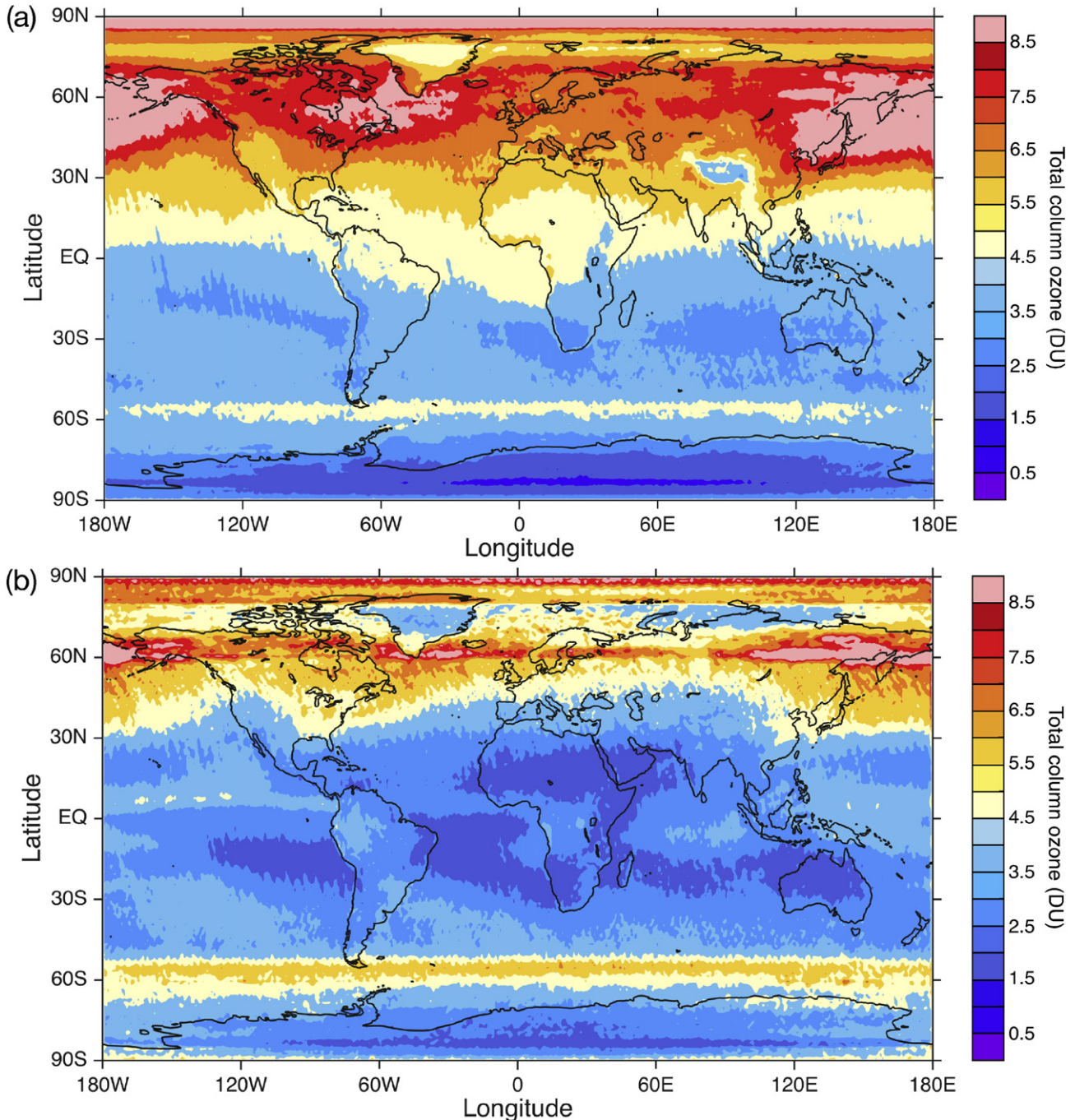


**Fig. 5.** Mean absolute bias (a) and associated standard deviation (b) of the relative bias between OMPS and OMI TCO observations during 2012–2015. The relative bias was calculated as TCO from OMPS minus those from OMI (abbreviated as OMPS-OMI in this context).

## 2.1. OMPS total ozone data

OMPS was launched on October 28, 2011, on board the S-NPP satellite. The instrumental suite is the latest space-borne ozone mapping instrument specifically designed to measure the total column and the vertical distribution of ozone on a daily basis for extending the nearly 40-year long-term global ozone records documented by previous backscatter UV sensors. OMPS is an advanced suite of three hyperspectral instruments that measure ozone by collecting sunlight in the UV and visible (VIS) ranges backscattered from the Earth's atmosphere. The sensor suite consists of a Total Column Nadir Mapper (TC-NM) that maps TCO with an approximate ground resolution of 50 km, a Nadir Profiler (NP) that measures ozone vertical profiles and a Limb Profiler (LP) that measures vertical ozone distribution in the lower stratosphere and troposphere with a vertical resolution of 1–3 km (Kramarova et al., 2014).

The OMPS detectors are two-dimensional charge-coupled devices (CCDs) and focal plane arrays, each arranged in one spectral and one spatial dimension. The TC-NM sensor uses a single grating spectrometer and a CCD array detector to measure backscattered radiance every 0.42 nm from 300 to 380 nm with 1.0 nm full width at half maximum (FWHM) resolution. The sensor has a 110° cross-track field-of-view (FOV) and a 0.27° along-track slit width corresponding to a 50 km resolution at nadir across a 2800 km swath. The 400 swaths per orbit with 36 across-track measurements per swath allow the TC-NM sensor to cover the entire globe daily (Flynn, Hornstein, & Hilsenrath, 2004). The OMPS NP sensor employs a double monochromator and a CCD array detector to make measurements every 0.42 nm from 250 to 310 nm with 1.1 nm FWHM resolution. The profiler has a 16.6° cross-track FOV and a 0.26° along-track slit width, yielding a 250 km by 250 km cell size synchronized with 5 center cells of the TC-NM. The OMPS LP sensor has a focal plane operating from 290 to 1000 nm for high vertical resolution ozone profile observations. The LP sensor has three vertical slits separated by 4.25° (across track) over the nominal 19 reporting-periods and makes about 160–180 measurements per orbit with 14 orbits per day, allowing a full global coverage every 3–4 days. Each slit has a 1.95° (112 km) vertical by 0.03° (2 km) horizontal FOV equating to 0–60 km coverage (Kramarova et al., 2014).

TCO observations from OMPS TC-NM used in this study were generated by NASA's OMPS science team with the latest SBUV V8.6 algorithm, a profile retrieval algorithm applied to SBUV type instruments, similar to the V8 algorithm used at NOAA for producing their operational

ozone products. TCO from SBUV type instruments is derived by integrating the retrieved profile, rather than from a separate set of wavelengths, as was applied in previous algorithms. Comparisons between V8.6 and V8 algorithms were detailed in Bhartia et al. (2013). Major changes are summarized as follows: 1) updates to instrument calibration process; 2) incorporation of new ozone absorption cross-sections in the forward model; the Malicet et al. (1995) ozone absorption cross-sections were applied in V8.6 instead of those from Bass and Paur (1985) used in V8; and 3) inclusion of new ozone and cloud height climatologies; in V8.6, a monthly latitudinal climatology of temperatures developed from NOAA temperature datasets were used to minimize biases from the variation of the ozone cross-section with the temperature. The cloud pressure climatology was based on the optical centroid pressure derived from rotational Raman scattering using OMI data.

Performance of OMPS TCO products was fully evaluated after a 3-year operational period in the orbit. With the early 14-month V8.6 TCO products from OMPS, Bai, Liu, Shi, and Gao (2015) observed a mean positive bias of ~1% in comparison with the collocated ground-based TCO measurements from 34 Brewer and 39 Dobson spectrophotometers; no apparent bias was observed with time, latitude, solar zenith angle (SZA), viewing geometry, or cloud fraction. By contrast, a negative bias of 2–4% was observed from the NOAA operational V8 TCO products (Flynn et al., 2014). Other relevant works evaluating the performance of OMPS can be found in the literature (e.g. Seftor et al., 2014; Wu et al., 2014). Daily Level-3 gridded TCO product derived from the V8.6 algorithm over the 2012–2015 period (Table 1) was applied in this study.

## 2.2. OMI TCO data

OMI is a nadir viewing and wide swath UV–visible hyperspectral spectrometer on board the NASA EOS-Aura satellite launched on 15 July 2004 (Levelt et al., 2006). It measures reflected and backscattered solar light from the Earth's atmosphere and surface in the wavelength range from 270 to 370 nm (UV) and 350–500 nm (VIS) with a spectral resolution of 0.45 nm in the UV and 0.63 nm in the VIS. The UV channel is further divided into UV-1 and UV-2 sub-channels at about 310 nm. The channel has a ground swath of 2600 km with each swath having 60 and 30 cross-track pixels for UV-2/VIS and UV-1 spectra. The ground pixel size at nadir is 24 km (UV-2/VIS) and 48 km (UV-1) in the across-track direction and 13 km in the flight direction. The mission of OMI is to provide daily global TCO measurements to continue the TCO record

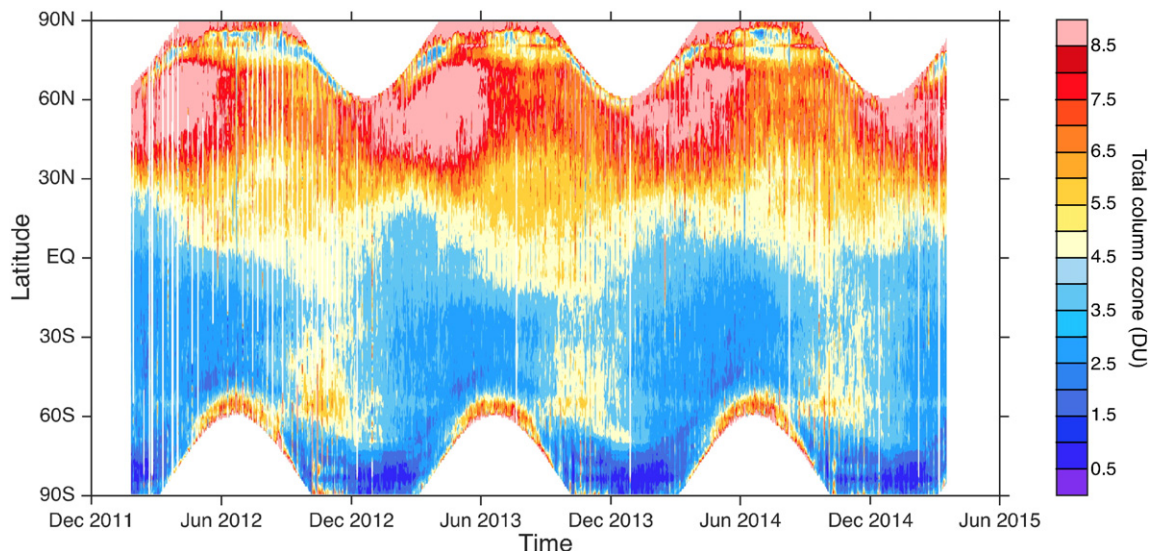


Fig. 6. Daily zonal mean absolute TCO bias between OMPS and OMI during 2012–2015.

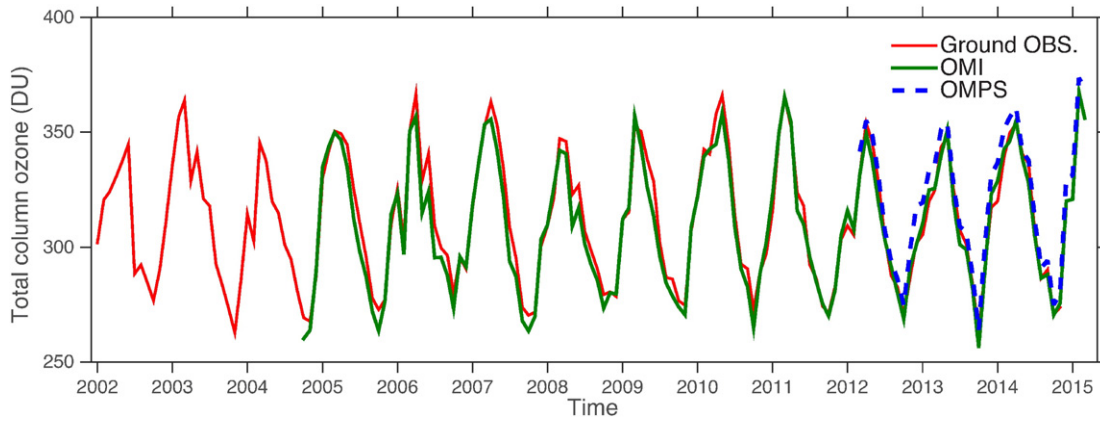


Fig. 7. Comparison of monthly TCO between satellite observations and collocated ground-based measurements at the TSUKUBA station.

established by the NASA Total Ozone Mapping Spectrometer (TOMS) series of instruments since 1978.

In calculating the total ozone, OMI provides two different TCO products by applying OMI-TOMS and Differential Optical Absorption

Spectroscopy (OMI-DOAS) retrieval algorithms, respectively. The OMI-TOMS TCO products are based on the long-standing TOMS V8 retrieval algorithm (Bhartia & Wellemeyer, 2002). The TOMS algorithm uses sun-normalized radiances at paired wavelengths (317.5 nm and

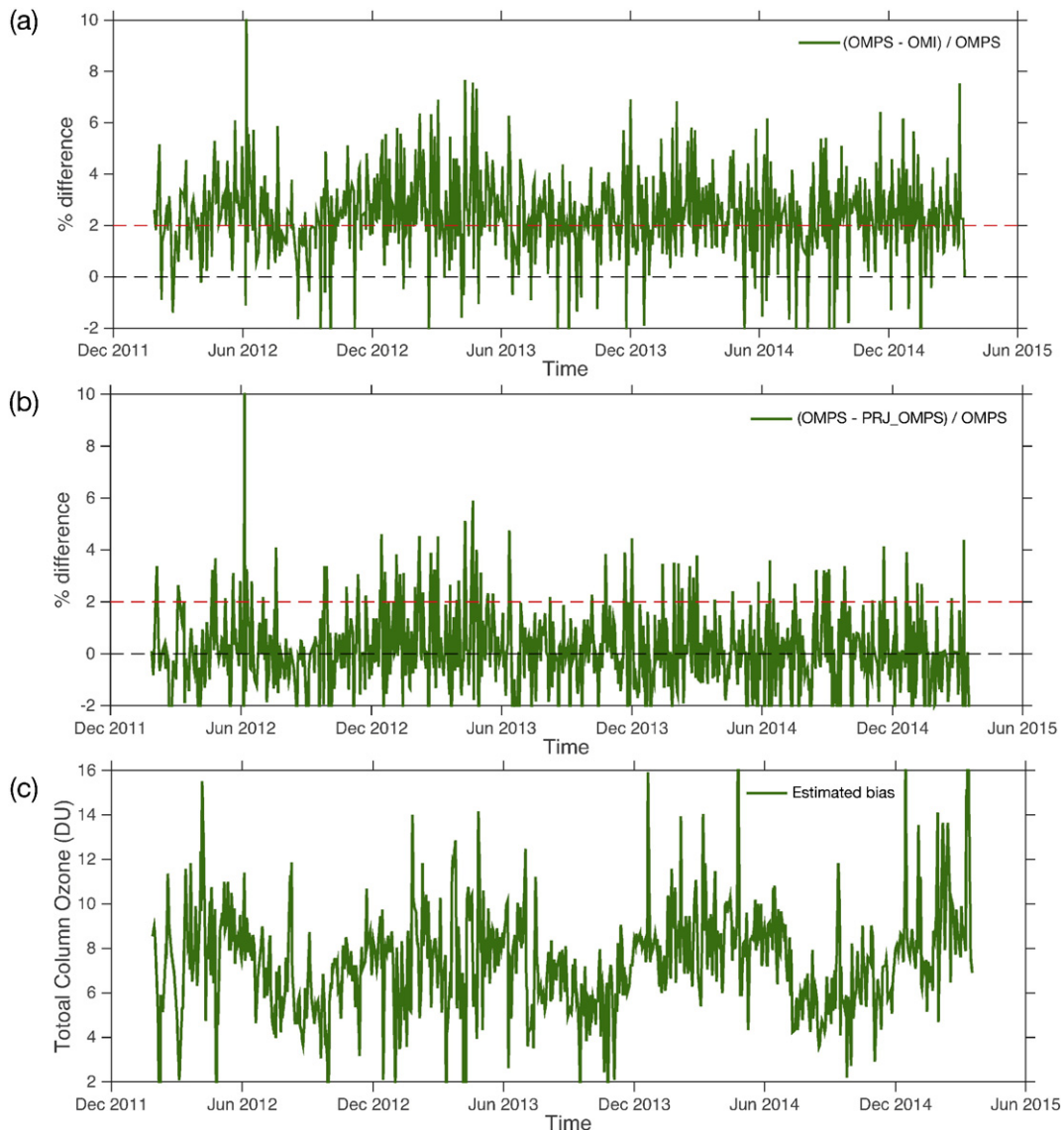


Fig. 8. Comparison of daily percent difference between OMPS and OMI at the TSUKUBA station before and after bias correction. (a) before bias correction, (b) after bias correction, (c) estimated cross-mission bias between OMPS and OMI.

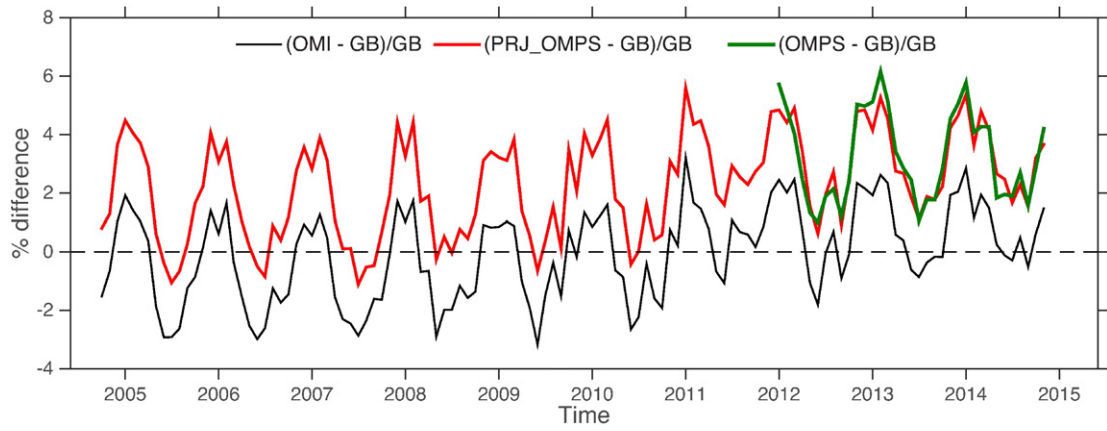


Fig. 9. Comparisons of monthly mean relative differences between satellite and ground-based TCO observations at the TSUKUBA station before and after bias correction.

331.2 nm under most conditions, and 331.2 nm and 360 nm for high ozone and high SZA conditions, respectively) for ozone retrieval. The essence is based on different absorption of ozone at two wavelengths because one is significantly absorbed by ozone whereas the other is insensitive. The OMI-DOAS retrieval algorithm was specifically developed for OMI. With this algorithm, TCO is estimated in three steps (Veefkind, De Haan, Brinksma, Kroon, & Levelt, 2006). First, the slant column density of ozone is calculated with the actual DOAS-based fitting of the measured spectrum in the spectral range of 331.2–336 nm. This slant column density is the amount of ozone along an average photon path from the sun, through the atmosphere, to the satellite. Second, the vertical column density of ozone is estimated by dividing the slant column density with the air mass factor. Finally, the initial estimates of vertical column are further corrected for cloud contaminations.

Performance of TCO products derived from both algorithms have been fully evaluated. By comparing with globally distributed ground-based Brewer and Dobson spectrophotometers TCO measurements, an averaged agreement of  $\sim 1\%$  for OMI-TOMS and  $\sim 2\%$  for OMI-DOAS data were observed, respectively (Balis et al., 2007). As suggested, the OMI-TOMS TCO products were observed to have high overall accuracy with no significant dependence on latitude or SZA. The OMI-DOAS data products were observed to have no significant dependence on latitude except at the high latitudes in the SH, where the OMI-DOAS systematically overestimated the ground-based TCO measurements. By comparison, a significant dependence on SZA was observed between OMI-DOAS and ground-based TCO measurements. Moreover, a seasonal dependent bias was observed and was further confirmed by Bak et al. (2015), in which an average  $\sim 1.65\%$  underestimation of OMI-TOMS and OMI-DOAS compared with collocated Brewer measurements was reported. Similar results can also be found in Antón et al. (2009), indicating a  $\sim 2\%$  underestimation by OMI-TOMS relative to 1.4% by OMI-DOAS. A more significant seasonal dependent bias between OMI-DOAS and Brewer measurements than that of OMI-TOMS necessitates further bias correction.

In this study, the OMI-TOMS daily Level-3 gridded TCO product (OMTO3d) was employed. This product, the ensemble of all Level-2 ground pixels with pixel centers having the same local calendar date on the ground, was generated by the NASA OMI science team by gridding only high quality Level-2 TCO orbital swath data on a 1 by 1° grid as weighted average. During the gridding process, a variety of quality control criteria were established and implemented, such as the exclusion of Level-2 observations with the solar eclipse possibility flag, row anomaly flag, and others, to attain an accuracy-assured TCO estimation. To illustrate the possible influence of cross-mission biases on the long-term trend estimation, OMI-TOMS TCO observations during 2004–2015 were all applied.

### 2.3. Ground-based TCO data

To date, TCO measurements from the well-established World Meteorological Organization/Global Atmosphere Watch (WMO/GAW) network routinely archived at the WOUDC have been widely used as ground-based references (Balis et al., 2007). TCO measurements from Brewer and Dobson spectrophotometers are commonly applied to validate satellite TCO observations. Both Brewer and Dobson instruments measure TCO in the atmosphere by observing spectral irradiance of solar radiation at specific wavelengths, which mainly rely on the theory of differential absorption in the Huggins band in the UV spectrum where ozone exhibits strong absorption features (Brewer, 1973; Dobson, 1968). The Dobson spectrophotometer is a large and manually controlled two-beam instrument that measures TCO relying on the ratio of the direct sunlight intensities at two standard wavelengths. Based on the selected slits, the instrument compares spectral irradiances of solar radiation at the three wavelength pairs A, C, D in the UV part of the spectrum with strong and weak absorption by ozone (A:305.5/325.4, C: 311.5/332.4, D: 317.5/339.9 nm). The most widely used combination is the AD double-pair of 305.5 nm/325.4 nm and 317.6 nm/339.8 nm. The Brewer spectrophotometer works similarly to the Dobson but is fully automated and has an improved optical design. TCO values of the Brewer are determined by taking the ratio of sunlight

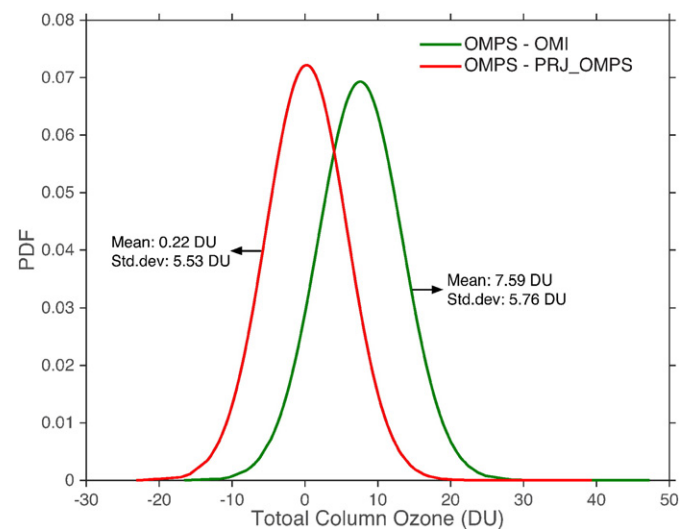


Fig. 10. Comparisons of probability density function (PDF) of TCO differences (OMPS-OMI) between OMPS and OMI at the TSUKUBA station before and after bias correction.

intensities at four wavelengths (306–320 nm) with a resolution of 0.6 nm to overcome the spectral interference of sulfur dioxide with ozone.

Accuracies of TCO recorded by Brewer and Dobson instruments are well documented. A well-maintained and calibrated Dobson instrument measures TCO with an estimated accuracy of 1% for direct sun observations and 2–3% for zenith sky or for SZA < 75° (Basher, 1982). Similarly, a well-calibrated Brewer instrument has an error level comparable to the Dobson instrument, with an estimated accuracy of 1% through direct sun observations (Antón et al., 2009). Despite the similarity in performance between the Brewer and Dobson instruments, a small difference within  $\pm 0.6\%$  was still observed due to the use of different wavelengths and varying temperature dependences for the ozone absorption coefficients (Van Roozendaal et al., 1998). Daily TCO products recorded by 38 well-maintained Dobson spectrophotometers from the WOUDC archive during 2004–2015 were employed as ground truth in this study (Fig. 2).

To guarantee fair comparisons, only ground-based TCO measurements under direct-sun and blue-sky observation mode were applied.

### 3. Methodology

#### 3.1. Bias correction method

##### 3.1.1. Quantile-quantile adjustment

As suggested by Teutschbein and Seibert (2013), higher-skill methods such as distribution mapping perform better than simple methods such as the delta-change and linear scaling in addressing cross-platform biases. In this study, a modified bias correction method was proposed based on one statistical bias correction method, quantile-quantile (Q-Q) adjustment, originally developed to calibrate the projected regional climate model (RCMs) outputs to the observed local observations (Amengual, Homar, Romero, Alonso, & Ramis,

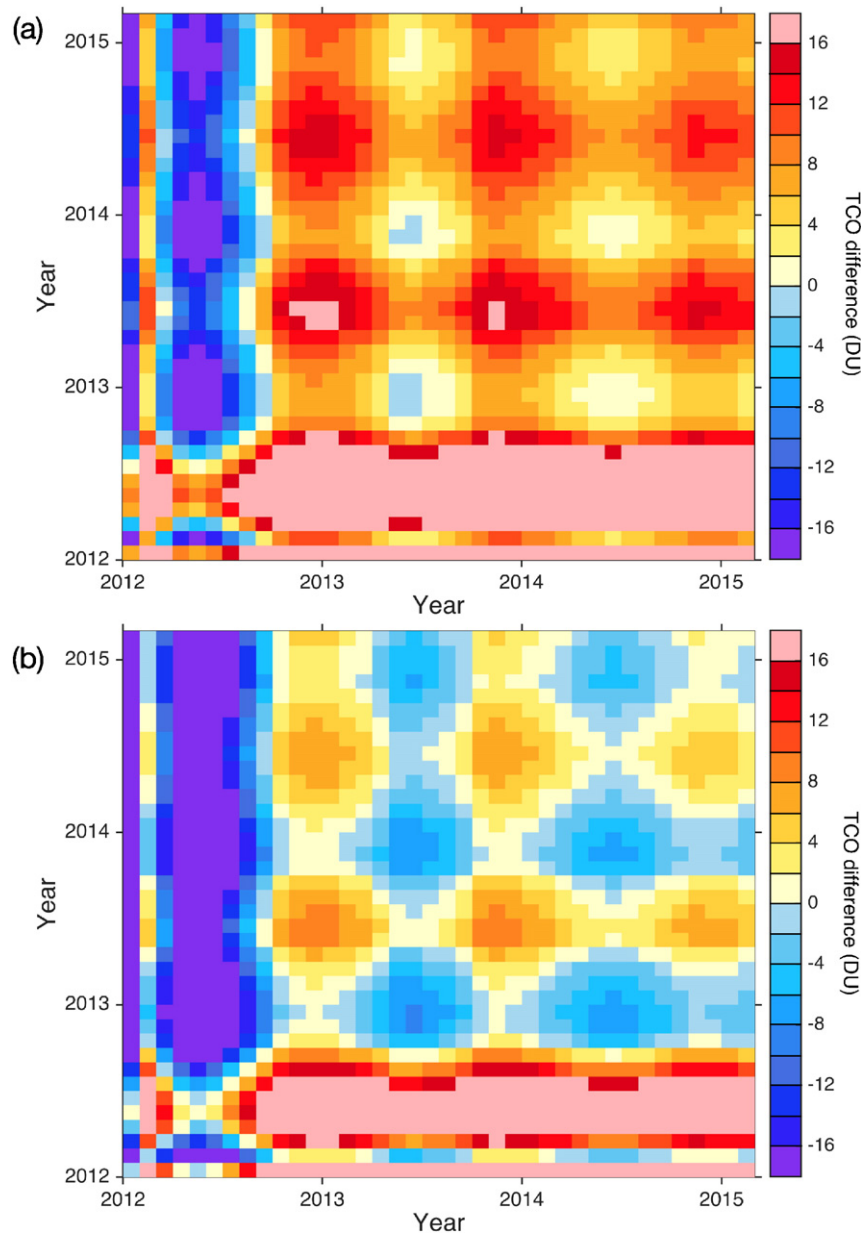


**Fig. 11.** Monthly cascade TCO differences (OMPS-OMI) (a) before and (b) after bias correction at the TSUKUBA station. The monthly cascade TCO differences indicate differences between TCO from OMPS and OMI over different months, and the diagonal elements thus represent TCO differences over the same months. The pixel value at the lower left corner represents the TCO difference between OMPS and OMI during January whereas the second pixel in the same row represent difference between TCO from OMPS during February and that of OMI during January.

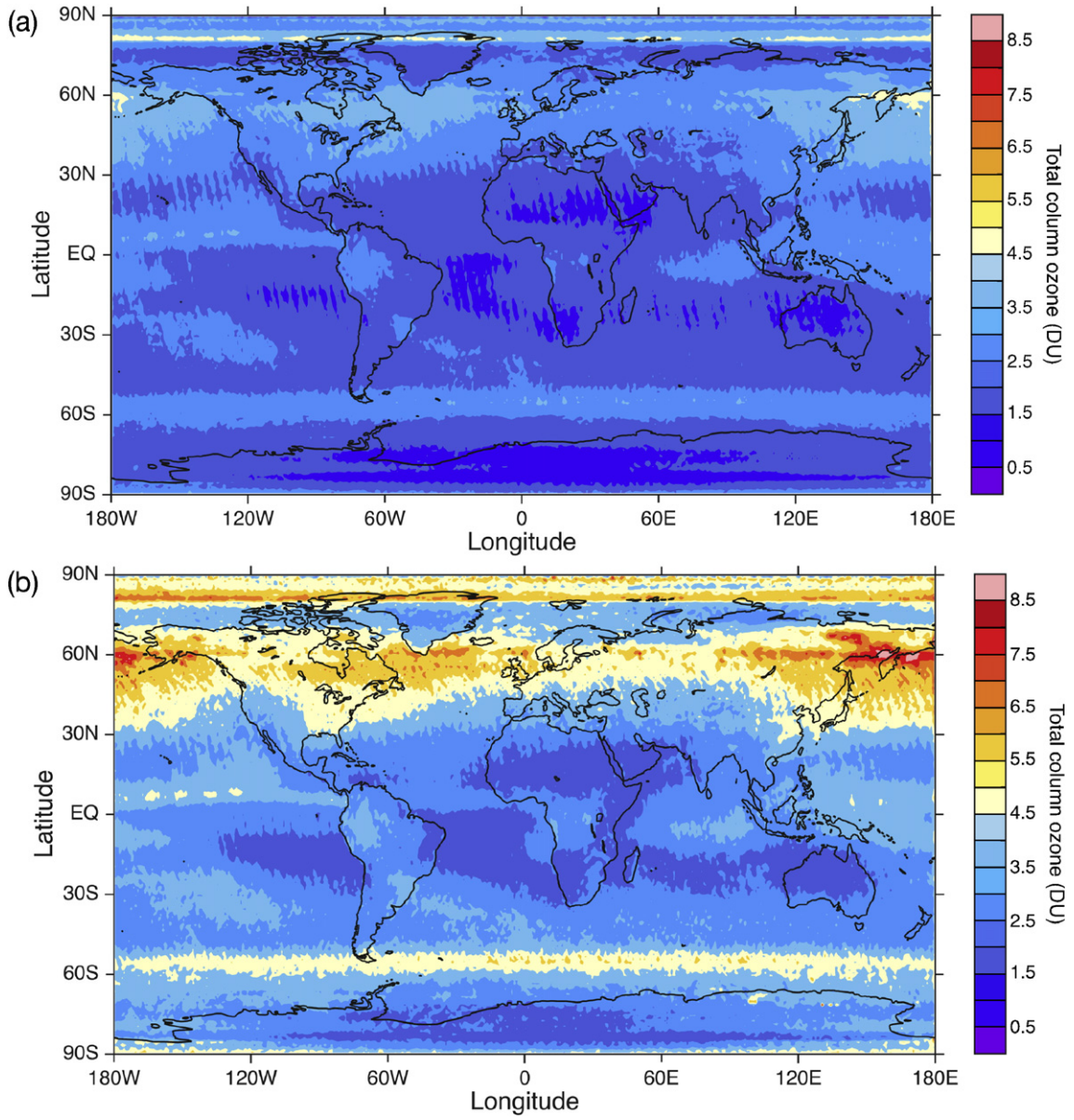


Fig. 12. Mean absolute bias (a) and (b) standard deviation of relative bias between OMPS and bias-corrected OMI TCO observations during 2012–2015.

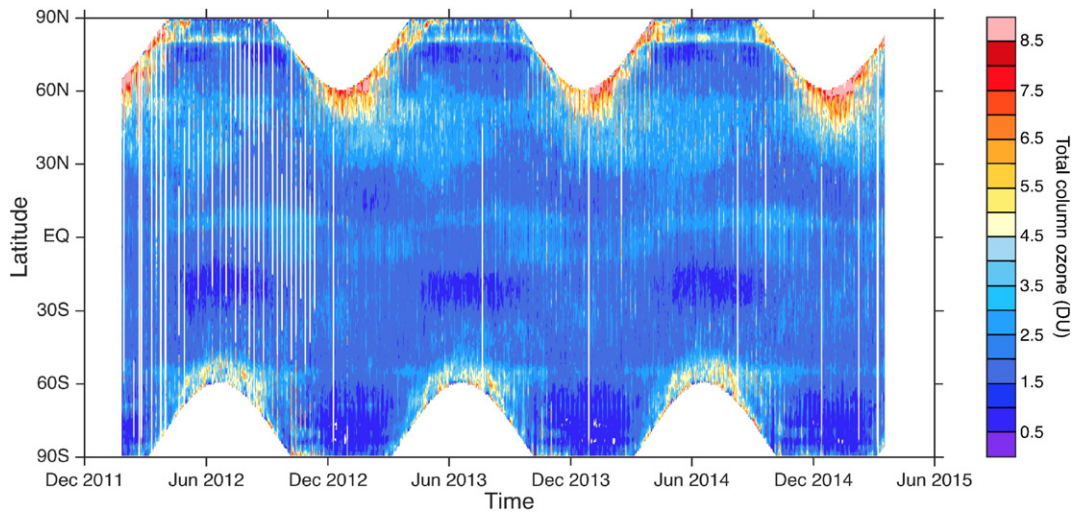


Fig. 13. Zonal mean absolute bias between OMPS and bias-corrected OMI total ozone observations during 2012–2015.

2011). The original Q-Q adjustment method relies on detecting changes in the cumulative distribution functions (CDFs) between the recent past observations and RCMs simulation outputs to characterize biases for calibrating future projections, a process referred to as distribution mapping. First, differences between CDFs of the recent past observed and simulated outputs of climate scenarios are detected. The projected regional climate models are then calibrated by removing the associated difference (or bias) for each prediction. In this step, the associated bias of a designated value in one projected time series is estimated based on the relevant difference between the recent past observed and simulated time series with the same percentile as shown in CDFs of the projected one. After this type of Q-Q adjustment, the projected climate scenarios are calibrated to the observed scenario standard because model biases have been removed. This method has proved effective in calibrating model projections of climate parameters, such as air temperature (Gerechuluun & Ahn, 2014) and precipitation (Osca, Romero, & Alonso, 2013). Results from these studies indicate that the accuracy of the calibrated outputs is significantly improved. An example depicting the principles of Q-Q adjustment for bias correction is shown in Fig. 3.

To merge TCO observations from OMPS and OMI toward a long-term coherent record, TCO observations from one sensor should be calibrated to another sensor's level by removing associated cross-mission biases between the two datasets. In the current study, TCO observations from OMI were calibrated to the OMPS level. In this context, OMPS was regarded as the baseline satellite sensor and OMI was viewed as the complementary satellite sensor. Reasons for this selection are detailed in Section 3.2.

As stated earlier, the original adjustment method requires all the input time series to have the same number of samples (e.g., same time scale: 3 years in Fig. 3) to guarantee accurate distribution mapping. In other words, to calibrate one time series with 3 years of observations, a length of 3 years common observations should also be guaranteed. To calibrate OMI observations to OMPS level during 2004–2007, the same number of control observations should be available as a reference basis to support such calibration (i.e., 3 years of 2012–2015 in this study) (Fig. 3). A TCO value,  $obs_j$ , in one observed OMI time series (black line in Fig. 3, defined as raw observation; OMI observation denoted as  $obs_{OMI}$  hereafter) can be calibrated to the OMPS level (dashed line

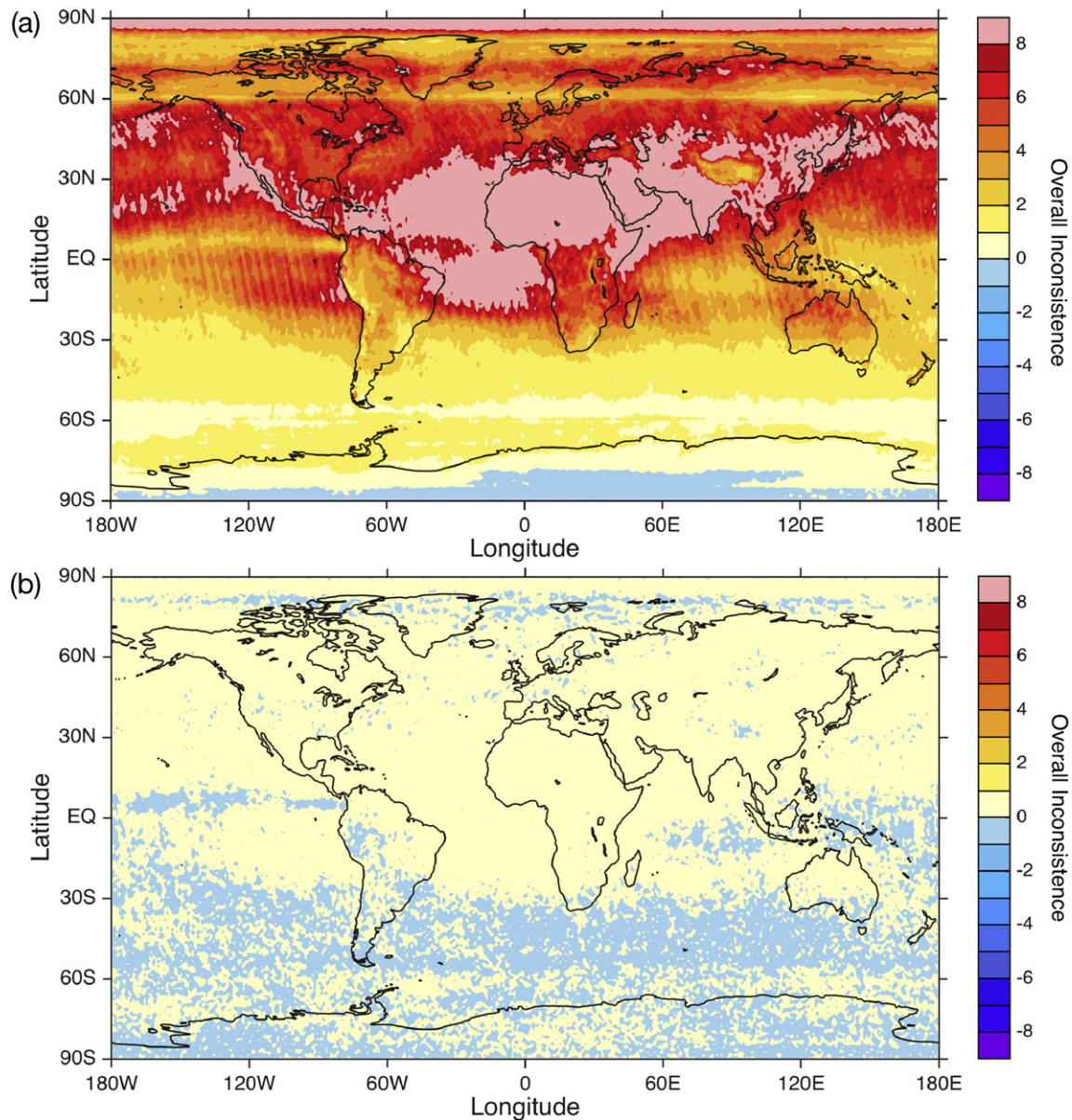
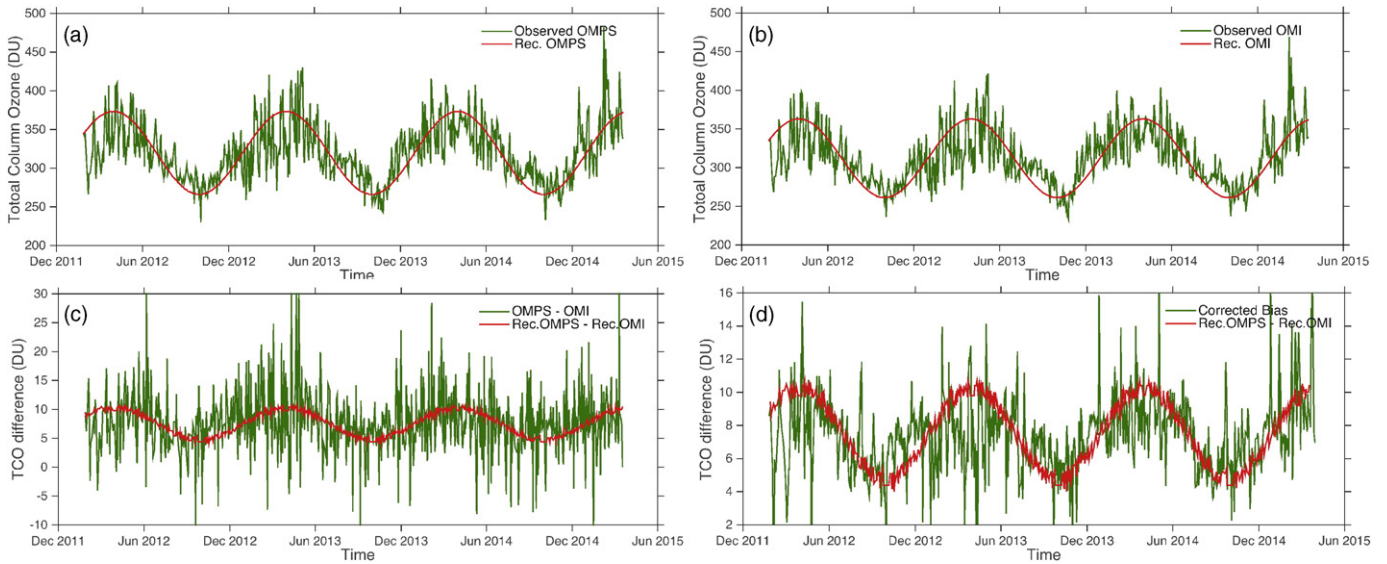


Fig. 14. Comparisons of the overall inconsistency (OI) between OMPS and OMI total ozone observations during 2012–2015. (a): OI between OMPS and OMI; (b) OI between OMPS and bias-corrected OMI.



**Fig. 15.** Comparisons between observed and reconstructed TCO at the TSUKUBA station. (a) comparisons of TCO between observations from OMPs (green) and the reconstructed one (red); (b) same as in (a) but for OMI; (c) comparisons of TCO differences between observations (i.e., OMPs-OMI) and that of a reconstructed one (i.e., Rec. OMPs - Rec. OMI); (d) comparisons of TCO differences between estimated biases from proposed bias correction algorithm (i.e., Corrected Bias) and that of reconstructed TCO differences. (Readers may refer to the web version of this diagram for the color representation of the two time series plots in this diagram.)

**Table 2**

Linear trends estimated from different TCO records at 38 ground-based stations. WMO ID: identifying number in WMO ground-based station network. Latitude: north positive. Longitude: east positive. N: number of months. OMI: untreated monthly TCO time series from OMI observations during 2004–2015. OMI + OMPs: merged monthly TCO time series between untreated OMI (2004–2012) and OMPs (2012–2015). PRJ\_OMP + OMPs: merged monthly TCO time series between bias-corrected OMI (i.e., PRJ\_OMP, 2004–2012) and OMPs (2012–2015). Ground-based: monthly TCO time series from ground-based measurements coincident with that of satellite observations.

WMO ID	Latitude	Longitude	N	OMI DU/month	OMI + OMPs DU/month	PRJ_OMP + OMPs DU/month	Ground-based DU/month
2	22.8	5.5	120	0.035	0.089	0.037	0.068
12	43.1	141.3	122	-0.085	0.005	-0.081	-0.094
14	36.1	140.1	122	0.023	0.097	0.023	-0.032
19	46.77	-100.75	113	0.170	0.240	0.177	0.199
27	-27.42	153.12	109	0.048	0.077	0.054	0.032
29	-54.5	158.97	108	0.077	0.096	0.077	-0.008
40	43.93	5.7	102	0.154	0.235	0.166	0.054
43	60.1	-1.2	103	0.133	0.208	0.149	0.113
51	64.1	-21.9	91	0.213	0.321	0.226	0.244
67	40.03	-105.25	117	0.081	0.128	0.082	0.077
68	51.84	20.79	111	-0.035	0.025	-0.032	-0.054
84	-12.42	130.88	109	0.043	0.073	0.049	0.032
91	-34.58	-58.48	110	0.046	0.076	0.050	-0.003
96	50.2	15.8	116	0.027	0.089	0.032	0.031
99	47.8	11	122	0.002	0.055	0.003	-0.014
101	-69	39.6	92	0.257	0.278	0.247	0.206
105	64.82	-147.87	78	-0.058	0.063	-0.044	0.183
106	36.25	-86.57	114	0.073	0.135	0.076	-0.001
107	37.93	-75.48	106	0.070	0.152	0.073	-0.110
111	-89.98	-24.8	52	0.627	0.606	0.651	0.690
152	30.1	31.3	105	0.051	0.125	0.055	0.076
159	-31.92	115.95	98	-0.018	0.014	-0.017	-0.066
190	26.2	127.7	120	0.032	0.084	0.032	0.033
191	-14.25	-170.56	83	0.126	0.163	0.129	0.064
199	71.32	-156.6	57	0.066	0.234	0.075	0.239
208	40	116.4	119	-0.049	0.030	-0.047	-0.132
209	25.03	102.68	83	0.057	0.140	0.058	0.077
214	1.33	103.88	70	0.001	0.021	0.000	0.087
216	13.67	100.61	119	0.033	0.081	0.036	0.034
219	-5.84	-35.21	24	0.439	0.439	0.477	-0.053
233	-64.23	-56.62	79	0.192	0.228	0.188	0.232
245	23.97	32.78	118	0.035	0.094	0.037	0.105
256	-45.03	169.68	104	0.014	0.043	0.011	-0.039
265	-25.91	28.21	95	0.122	0.141	0.127	0.137
268	-77.83	166.67	69	0.306	0.344	0.309	0.310
284	64.2	19.8	79	-0.269	-0.162	-0.266	-0.186
293	38	23.7	120	-0.034	0.033	-0.030	-0.058
339	-54.85	-68.28	109	0.064	0.087	0.069	0.097
Average				0.081	0.136	0.086	0.068

in Fig. 3, defined as projected OMPS time series; denoted as  $prj_j$ ) by removing the associated bias. This process is modeled as:

$$prj_j = obs_j + \Delta TCO_j \quad (1)$$

where  $prj_j$  denotes the projected TCO value at the OMPS level;  $obs_j$  is the  $j$ th value in the raw observation time series; and  $\Delta TCO_j$  is the relevant bias between OMPS and OMI at the given  $obs_j$ .

Following the principles of Q-Q adjustment,  $\Delta TCO_j$  can be estimated through distribution mapping between common TCO observations of OMPS and OMI during the overlapped time period of 2012–2015. Here, these common observations are defined as two control observations, which can be denoted as  $C_{OMPS}$  and  $C_{OMI}$ , respectively. The collective calibration processes are formulated as:

$$\Delta TCO_j = g\bar{\Delta} + f\Delta'_i \quad (2)$$

where

$$i = p_1 | obs_{OMI} \approx obs_j \quad (3)$$

$$\Delta_i = C_{OMPS}^i - C_{OMI}^i \quad (4)$$

$$\bar{\Delta} = \frac{1}{N} \sum \Delta_i = \overline{C_{OMPS}} - \overline{C_{OMI}} \quad (5)$$

$$\Delta'_i = \Delta_i - \bar{\Delta} \quad (6)$$

$$g = \frac{\overline{obs_{OMI}}}{\overline{C_{OMI}}} \quad (7)$$

$$f = \frac{IQR_{obs_{OMI}}}{IQR_{C_{OMI}}} \quad (8)$$

$$IQR_{obs_{OMI}} = obs_{OMI}|_{p=75\%} - obs_{OMI}|_{p=25\%} \quad (9)$$

$$IQR_{C_{OMI}} = C_{OMI}|_{p=75\%} - C_{OMI}|_{p=25\%} \quad (10)$$

In Eqs. 2–6,  $p_1$  denotes the associated CDFs of  $obs_{OMI}$  (i.e., raw observations of OMI);  $i$  is the associated percentile of  $obs_j$  in  $p_1$ ;  $N$  is the number of samples in the raw observation time series;  $\overline{C_{OMPS}}$  and  $\overline{C_{OMI}}$  denote the mean value of  $C_{OMPS}$  and  $C_{OMI}$ , respectively;  $g$  and  $f$  are two modulation parameters; and  $IQR_{obs_{OMI}}$  and  $IQR_{C_{OMI}}$  are the interquartile range of raw and control TCO observations from OMI at 75% and 25% percentile.

As shown in Eqs. 2–10, estimated biases are highly dependent on the CDFs of raw observation and two control TCO observations, meaning that the raw observation and two control time series should have the same number of samples. For instance, to calibrate an observed 10-year TCO time series from OMI, two 10-year overlapped TCO time series from OMPS and OMI must be prepared as control observations to guarantee accurate distribution mapping. Otherwise, biases might not be fully addressed, especially for those biases with dependence effects. This constraint limits the application of the original method to other cases, especially for removing cross-mission biases between satellite

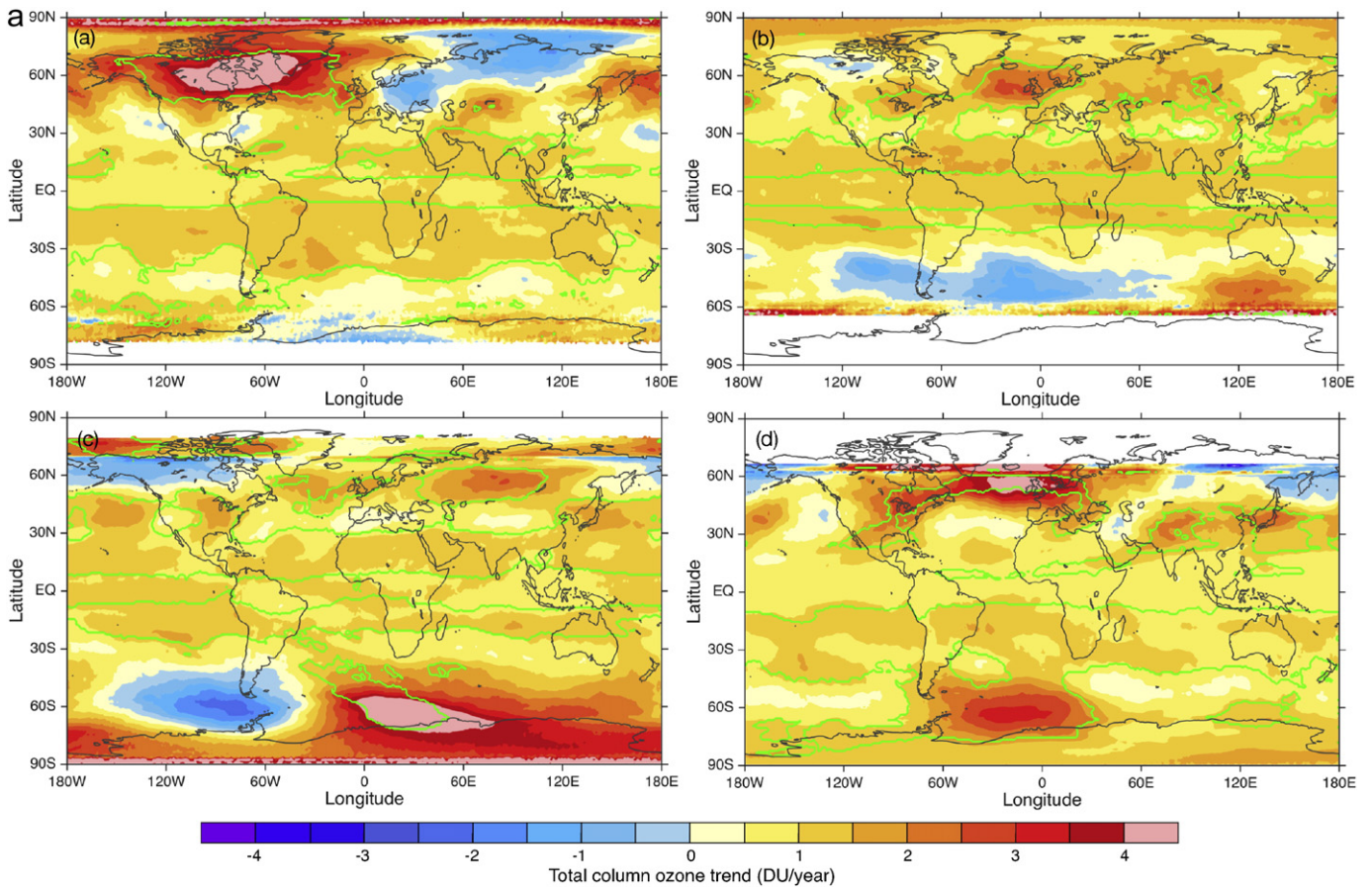


**Fig. 16.** a. Panel a is comprised of four subdiagrams on the top of this diagram. Seasonal TCO trends derived from the merged OMI and OMPS observations during 2004–2015. (a): spring (MAM), (b): summer (JJA), (c): fall (SON), (d): winter (DJF). Trends are represented by slope of the fitted straight line to each merged TCO time series (i.e., linear fitting). Green contour lines depict regions where trends are significant at the 90% confidence interval. White area indicates no trend estimation due to the lack of reliable TCO observations. b. Panel b is comprised of four subdiagrams at the bottom of this diagram. Same as Fig. 16a (Panel a) but trends derived from the merged TCO time series between bias-corrected OMI and OMPS.

observations, due to difficulties in attaining lengthy overlapped control observations.

3.1.2. Modified bias correction method

To address this temporal constraint in cross-mission data merging and improve applicability of the original method for cross-mission bias correction, some essential modifications are necessary to optimize the bias estimation process. The entire modified process to estimate cross-mission biases between OMI and OMPS (Fig. 4) can be summarized as follows:

- 1) Stage 1: Control observations of OMPS and OMI are generated from their common observations during the overlapped time period. To handle seasonal dependent cross-mission biases, control observations should have adequate samples that cover at least a full period cycle (e.g., one year for TCO). Generally, more accurate relationships can be characterized to estimate cross-mission biases with the higher number of samples in control observations. Therefore, in this study, all common observations of OMPS and OMI during 2012–2015 were used to generate the two relevant control observations.
- 2) Stage 2: Regardless of the number of samples included, any observed OMI TCO time series (i.e., raw observation) can be projected to the OMPS level by removing associated bias for each sample. For example, the  $\Delta TCO_j$  for  $obs_j$  in the raw observation time series of OMI can be estimated from:

$$\Delta TCO_j = g' \bar{\Delta} + f' \Delta'_{ii} \tag{11}$$

where

$$ii = p_2 |_{C_{OMI}=obs_j} \tag{12}$$

$$\Delta_{ii} = C_{OMPS}^{ii} - C_{OMI}^{ii} \tag{13}$$

$$\bar{\Delta} = \overline{\overline{C_{OMPS}}} - \overline{\overline{C_{OMI}}} \tag{14}$$

$$\Delta'_{ii} = \Delta_{ii} - \bar{\Delta} \tag{15}$$

$$g' = \frac{\overline{\overline{C_{OMPS}}}}{\overline{\overline{C_{OMI}}}} \tag{16}$$

$$f' = \frac{IQR_{C_{OMPS}}}{IQR_{C_{OMI}}} \tag{17}$$

$$IQR_{C_{OMPS}} = C_{OMPS}|_{p=75\%} - C_{OMPS}|_{p=25\%} \tag{18}$$

where  $p_2$  denotes the associated CDFs of  $C_{OMI}$  (i.e., control observations of OMI);  $ii$  is the  $i$ th percentile in  $p_2$  and is estimated by finding the data value  $C_{OMI}$  equal (or close) to the given observation  $obs_j$ ;  $\overline{\overline{C_{OMPS}}}$  and  $\overline{\overline{C_{OMI}}}$  denote the median value of the two control observations;  $g'$  and  $f'$  are two modulation parameters that adjust the distribution of the projected time series; and  $IQR_{C_{OMPS}}$  is the inter-quantile range of control TCO observations from OMPS at 75% and 25%.

The essence of this modified bias correction method is to estimate cross-mission bias individually for each sample in the raw observation time series, regardless of other samples and the distribution of the raw observation time series. Processes in Eqs. 11–18 can be interpreted

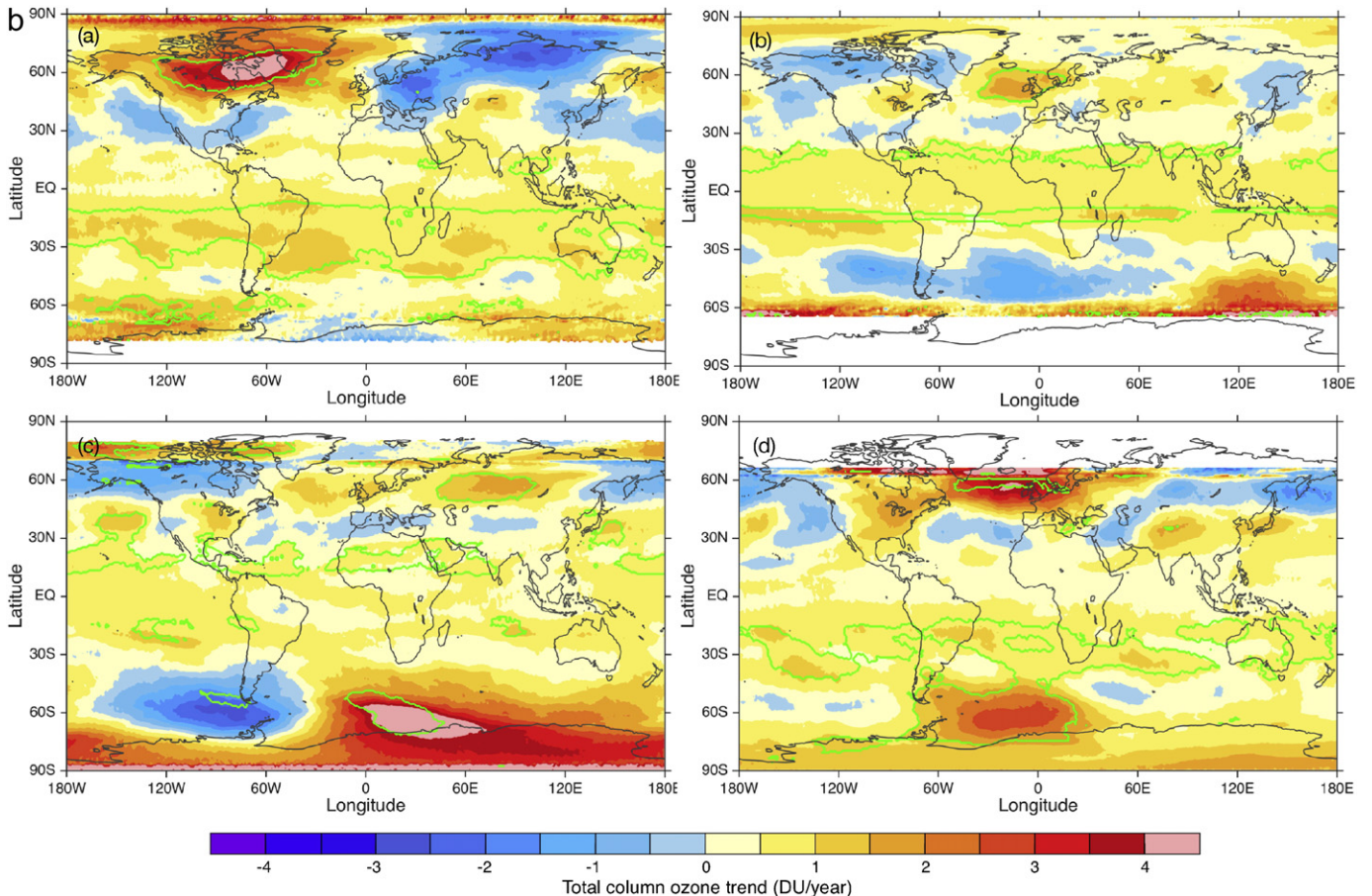


Fig. 16 (continued).

as: given any observed OMI TCO value (i.e.,  $obs_j$ ), the cross-mission bias toward this observation is only determined by the TCO value itself and distributions of two control observations. First, the associated percentile toward the given  $obs_j$  in the OMI control observation time series was estimated by finding the one with the same or closest data value to  $obs_j$  (Eq. 12). Once the percentile was determined, the relative data value with the same percentile in the OMPS control observation time series could also be obtained (i.e.,  $C_{OMPS}^i$ ). Second, the raw bias  $\Delta_j$  for the given  $obs_j$  can be estimated from Eq. 13. Finally, cross-mission bias toward the given  $obs_j$  (i.e.,  $\Delta TCO_j$ ) can be calculated through Eq. 11 because all other modulation parameters can be easily obtained from two control observation time series, unrelated to the given  $obs_j$ .

As indicated in Eqs. 11–18, the difference between the modified bias correction method and the original Q-Q adjustment lies in rationales for estimating biases. In the modified method, the median instead of the mean value was used to avoid error propagations due to possible large observation uncertainties. In addition, distribution mapping was only implemented between the two control observations (i.e.,  $C_{OMPS}$  and  $C_{OMI}$ ) without referring to the distribution of the raw observations (i.e.,  $obs$ ). Similarly, the two modulation parameters ( $g'$  and  $f'$ ) were also estimated only from two control observations. Within this context, the modified bias correction method may be more adaptive than the original one in bias characterization because it is independent from the probability distribution of the raw observations. This advancement enables the modified bias correction method to handle observations at different time scales and thus can be directly used to remove cross-mission biases between satellite observations.

### 3.2. Statistical bias correction scheme

By using the modified statistical bias correction method over each geographic grid (i.e., each pixel of remote sensing images), a long-term coherent TCO record can be created from OMI and OMPS observations at the global scale. Based on common observations between OMI and OMPS during the 2012–2015 overlapped time period, cross-mission biases were estimated and removed at each OMI geographic grid individually. As noted, OMPS was selected as the baseline satellite sensor for the creation of a long-term TCO record during the overlapped time period, despite OMI continuously providing TCO observations in the orbit during the same time period. The primary reason for this option is that OMPS will work in the orbit for the next 10 years whereas OMI will finish its mission in the upcoming years. Therefore, TCO observations from OMPS rather than those from OMI should be used as the baseline information to form the long-term record. With this merging scheme, the merged long-term TCO record can be updated simultaneously by directly incorporating the latest OMPS TCO observations without further bias correction in future. In this study, a long-term coherent TCO record was created by merging bias-corrected TCO observations from OMI during 2004–2012 with those from OMPS during 2012–2015.

As cross-mission TCO biases might have seasonal effects (e.g., Bak et al., 2015), monthly time series instead of observations through all seasons were used as control in the operational bias correction processes. This process means that, for example, to correct one OMI TCO value observed in January 2010 over one geographic grid, control observations for the estimation of associated cross-mission bias at this grid were

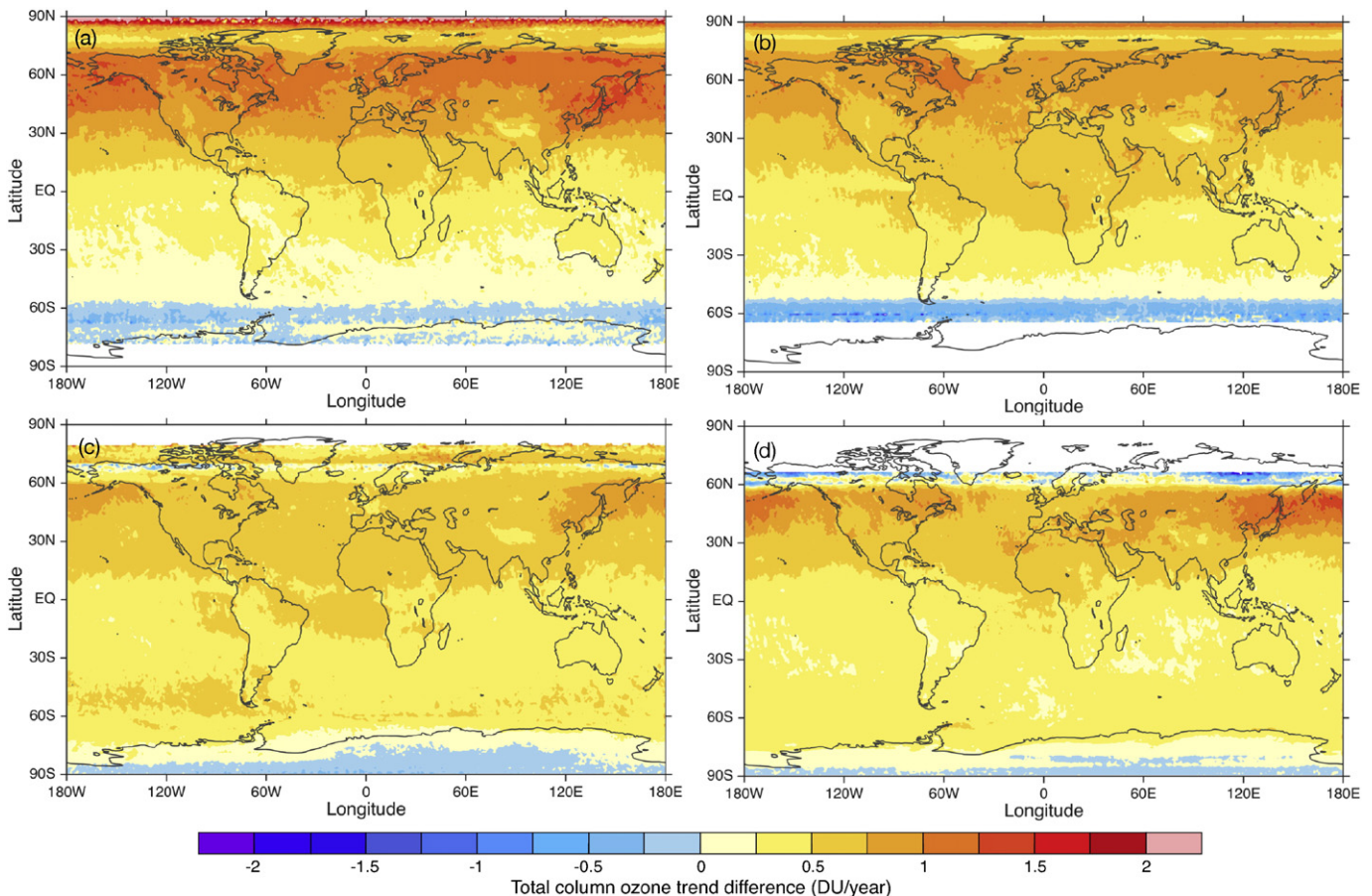


Fig. 17. Differences of seasonal TCO trends before (Fig. 16a) and after (Fig. 16b) bias correction. (a): spring (MAM), (b): summer (JJA), (c): fall (SON), (d): winter (DJF).

created only with TCO values observed in January from the common observations during the overlapped time period.

### 3.3. Overall inconsistency index

Adequate statistic indicators should be applied to evaluate the performance of the proposed bias correction method. In addition to the commonly applied mean relative difference (MRD) and root mean squared error (RMSE), one index termed as overall inconsistency (OI) was proposed based on the Mahalanobis distance ( $D_{Mah}$ ) to check the consistency (or similarity) between two time series. The  $D_{Mah}$  is one time series similarity measure that not only quantifies the difference between time series but also accounts for non-stationary of variance and temporal cross-correlation (Lhermitte, Verbesselt, Verstraeten, & Coppin, 2011; Mahalanobis, 1936). Because of the mathematical limitations (root squared), however, the  $D_{Mah}$  is incapable of reflecting the effect of overestimation and underestimation between time series and is prone to emphasize the mean squared root rather than the relative difference. To obtain a more comprehensive similarity between two time series, an improved time series similarity measure was proposed in this study by incorporating the MRD and mean absolute relative difference (MARD). Compared to the  $D_{Mah}$ , the OI not only emphasizes the overall difference between two time series but also indicates the overestimation (underestimation) through the positive (negative) sign of the calculated weights. These statistics were formulated as:

$$MRD = 100 \times \frac{1}{N} \sum_{i=1}^N \frac{SAT_i - GB_i}{GB_i} \quad (19)$$

$$MARD = 100 \times \frac{1}{N} \sum_{i=1}^N \left| \frac{SAT_i - GB_i}{GB_i} \right| \quad (20)$$

$$RMSE = 100 \times \sqrt{\frac{1}{N} \sum_{i=1}^N \left( \frac{SAT_i - GB_i}{GB_i} \right)^2} \quad (21)$$

$$D_{Mah} = \sqrt{\epsilon' \Sigma^{-1} \epsilon} \quad (22)$$

$$OI = MRD * \frac{RMSE}{MARD} * \frac{D_{Mah}^2}{N} \quad (23)$$

where  $SAT$  and  $GB$  denotes TCO observations from satellite and ground-based instruments, respectively;  $\epsilon$  is the error time series (i.e.,  $SAT-GB$ );  $\epsilon'$  stands for the transpose of the column vector  $\epsilon$ ;  $\Sigma$  is the error covariance matrix; and  $N$  is the number of samples in  $\epsilon$ . As suggested in Eq. 23, the range of OI is between  $-\infty$  and  $+\infty$ , with a perfect value of zero. A value of OI less than zero indicates underestimation, whereas a positive value implies overestimation.

## 4. Results

### 4.1. Bias correction

Apparent cross-mission biases were observed between overlapped OMPS and OMI TCO observations over the 2012–2015 period at the global scale (Figs. 5 and 6). The MARD (Fig. 5) indicates significant latitudinal dependent biases whereas the daily zonal mean (Fig. 6) shows apparent seasonal dependent biases. Large deviations were mainly observed at the mid-to-high latitudes in the Northern Hemisphere (NH), with most significant differences observed over the Arctic regions. In the time domain, larger deviations mainly occur during the boreal spring (i.e., March–April–May) in the NH, in which large TCO values were observed. Meanwhile, apparent biases were observed at the times close to the polar nights in the SH. This effect might be related to the low signal-to-noise ratio during those time periods due to the

viewing limitations (i.e., large SZA), and hence large uncertainties could be introduced into the derived total ozone products (Bai, Liu et al., 2015). Large uncertainties can also be deduced from large standard deviations of biases over those regions, however. In general, the cross-mission TCO biases between OMPS and OMI are spatiotemporal heterogeneous with nonlinear and non-stationary variability.

As described earlier, the modified bias correction method was applied to remove those observed complex cross-mission biases between OMPS and OMI TCO observations. Taking TCO observations recorded over the geographic grid where the TSUKUBA station (36.1°N/140.1°E) is located for example (Fig. 7), OMI slightly underestimated the TCO values whereas OMPS overestimated these TCO values relative to the collocated ground-based TCO measurements. Thus, differences between OMPS and OMI were much larger than those found by comparing them with the ground-based measurements individually. A mean positive bias >2% was observed between OMPS and OMI (Fig. 8a), from which apparent seasonal dependence can be observed as well. By applying the modified bias correction method, cross-mission biases were removed significantly between OMPS and OMI, with the remnant biases around zero (i.e., a mean bias around ~0.1%) (Fig. 8b). The estimated cross-mission biases through the modified bias correction method show significant seasonal effects (Fig. 8c). This chaotic bias time series suggests that the modified bias correction method is capable of addressing observed nonlinear and non-stationary time dependent biases. With this modified method, rather than removing a simple mean difference (e.g., delta-change) or a linear fitted value (e.g., linear transformation) from the raw observations, cross-mission biases were removed adaptively.

Performance of the proposed bias correction method was evaluated through different comparisons (Figs. 9–11). Vicarious comparisons of monthly MRD (Fig. 9) indicated fair agreements between OMPS and bias-corrected OMI TCO observations. Before bias correction, OMI underestimated ground-based TCO measurements by ~1% whereas OMPS overestimated by ~3% at the TSUKUBA station. Thus, distinct cross-mission biases were observed between OMPS and OMI at this geographic grid. Nevertheless, biases were reduced to a level of 0.1% after bias correction. In addition, the probability density functions (PDFs) of TCO differences between OMPS and OMI before and after bias correction were also compared (Fig. 10). As indicated, a mean positive bias of 7.6 DU was observed before bias correction, whereas it was reduced to 0.2 DU after correction. The standard deviation of biases was reduced as well after bias correction, reflecting the adaptive nature of the modified bias correction method.

To depict significant cross-mission biases between OMPS and OMI before bias correction and the performance of bias correction method, the monthly cascade differences were calculated as well (Fig. 11). Because TCO presents a sinusoid variability throughout the year due to seasonal variations, the monthly cascade differences should be positive and negative every three months. Nevertheless, it indicates significant cross-mission biases between OMPS and OMI before bias correction, from which seasonal behavior is barely detected (i.e., biases not shown with positive and negative alternatively in Fig. 11a). After bias correction, cross-mission biases were significantly reduced, represented by apparent seasonal variability of TCO differences (Fig. 11b). Compared to the original time series before bias correction, the projected OMI data are more consistent with OMPS, deduced not only from the TCO differences in the same month (i.e., diagonal values) but also from the more significant seasonal effects (i.e., positive and negative values alternatively) of the monthly TCO differences after bias correction (Fig. 11b).

Comparisons of TCO observations between OMPS and bias-corrected OMI (Figs. 12 and 13) are in the form of mean absolute bias at the global scale. This comparison shows that the apparent latitudinal and seasonal dependent cross-mission biases were significantly reduced, especially for the location at the mid-to-high latitudes in the NH during the boreal spring, where large cross-mission biases were observed before bias correction. Compared to the raw TCO time series, bias-corrected OMI was

more consistent with OMPS at the global scale, with a mean TCO difference <5 DU globally, except for regions over the 60°N–90°N due to large SZAs (Fig. 13). Despite some large standard deviations persisting after bias correction (Fig. 12b), they have been significantly reduced (Fig. 12b) compared to those before bias correction (Fig. 5b). Those remnant large standard deviations and biases indicate that large uncertainties could be introduced into the TCO retrieval process due to limited viewing conditions; however, removing those random biases with limited control observations is still difficult.

In addition to the mean absolute bias, the OI was also calculated to evaluate the consistency between OMPS and OMI TCO observations. OMPS has large values relative to OMI observations globally, with significant inconsistency ( $OI > 5$ ) observed in the NH, especially over the Arctic and tropic regions (Fig. 14a). It is indicative that large biases were present mainly at the mid-to-high latitudes in the NH and the Arctic regions (Figs. 5 and 6); thus, large OI values over these regions could be primarily attributed to the associated large cross-mission biases between OMPS and OMI at these locations. Nevertheless, significant inconsistencies were also observed in the tropic regions where small cross-mission TCO biases were observed. After comparing TCO observations between OMPS and OMI over the tropics, it can be found that the cross-mission biases between them were small in magnitude but with poor correlations. This effect demonstrates the advantage of OI compared to other simple parameters such as the MRD and RMSE, which only reflects deviations between time series without considering variance and correlation. Therefore, OI is more comprehensive and reliable for the evaluation of time series similarity as variances and correlations must also be considered. After bias correction, the apparent inconsistency was significantly removed, with an improvement of overall consistency by ~90% at the global scale (calculated from  $100 \times \frac{\frac{1}{N} \sum_{i=1}^N |OI_i^{before}| - \frac{1}{N} \sum_{i=1}^N |OI_i^{after}|}{\frac{1}{N} \sum_{i=1}^N |OI_i^{before}|}$ ). As indicated therein, an OI within  $\pm 1$  was observed over each geographic grid globally (Fig. 14b). Compared to the bias-corrected OMI TCO observations, the OMPS showed a slight overestimation in the NH and a negligible underestimation in the SH. Overall, the modified bias correction method worked well in removing those observed latitudinal and seasonal dependent biases between OMPS and OMI TCO observations.

To gain further insight into the estimated cross-mission TCO biases, raw OMPS and OMI TCO observations were reconstructed based on the time-dependent variability from two satellite time series observations during the overlapped time period. Time variable was defined as  $\sin(2\pi * DOY/365)$ , where the day-of-year (DOY) represents the observation date. First, CDFs of pair-wised satellite TCO observations and the associated time variables during the overlapped time period were calculated. TCO of OMPS and OMI were then reconstructed individually based on the time variable through the same concept of distribution mapping (Fig. 15). The reconstructed TCO time series clearly exhibited seasonal variability (Fig. 15a–b). Unlike the raw time series with large fluctuations, the reconstructed time series varied smoothly along the time horizon. Biases between these two reconstructed TCO time series were also compared with the original biases (i.e., OMPS–OMI in Fig. 15c) and the biases estimated from the proposed modified bias correction method (i.e., corrected bias in Fig. 15d), respectively. Results indicate that the cross-mission biases between OMPS and OMI were mainly dominated by the seasonal dependent biases, and the modified bias correction method not only removed the apparent seasonal dependent biases but also addressed some other random biases. Possible reasons for these observed cross-mission TCO biases have been investigated in the literature, such as in McPeters et al. (2013) and Frith et al. (2014).

#### 4.2. Impacts of cross-mission biases on trend analysis

Cross-mission biases not only caused apparent inconsistencies between TCO observations from OMI and OMPS in the time horizon but

also produced large uncertainties in long-term trend estimations, which in turn could result in an earlier expectation of ozone layer recovery at the global scale. To evaluate the possible impacts of cross-mission biases on trend analysis, linear trends estimated from the merged TCO time series before and after bias correction, represented by the slope of the fitted straight line to each time series, were compared. Monthly trends derived from the merged TCO record between OMI and OMPS at 38 ground-based stations were compared (Table 2). As references, trends derived from the untreated monthly OMI TCO time series and coincident ground-based TCO measurements during 2004–2015 were calculated. Results indicated that trends derived from the merged TCO time series without bias correction (i.e., OMI + OMPS) significantly overestimate those from other three datasets, including the bias-corrected (i.e., PRJ\_OMPS + OMPS) and the untreated OMI TCO time series, and the ground-based TCO measurements. An apparent increasing trend was observed from the simply merged TCO time series between OMPS and OMI without bias correction at 38 ground-based stations in the past decade, with a speed of 0.136 DU/month, almost twice those from the original OMI (0.081 DU/month), the bias-corrected OMI (0.086 DU/month), and the ground-based measurements (0.068 DU/month). Significant deviations between these estimated trends, especially toward the one derived from the merged TCO record without bias correction, showing a TCO increase rate twice that of the ground-based measurements, strongly demonstrate the necessity of bias correction prior to cross-mission data merging.

In addition to significant impacts on magnitudes of estimated trends, cross-mission biases can also result in different phases (i.e., opposite signs) of trends, such as the one at BELSK station (WMO/GAW ID: 68) (Table 2). An increasing trend (0.025 DU/month) was observed from the merged TCO time series without bias correction, whereas it indicates decreasing trends from the untreated OMI (–0.035 DU/month), bias-corrected (–0.032 DU/month), and ground-based (–0.054 DU/month) TCO time series. In contrast to changes in magnitudes to estimated trends, changes in phases of estimated trends were more serious in trend analysis because opposite projections will be conducted. Despite some inconsistency observed between the estimated satellite-based trends and that of ground-based measurements, the negligible differences between derived trends from the bias-corrected time series and untreated OMI time series clearly indicate that trends derived from the bias-corrected time series were more accurate than those without bias correction.

To further depict the impacts of cross-mission biases on trend analysis, seasonal TCO trends during 2004–2015 were estimated from the merged TCO time series before (Fig. 16a) and after (Fig. 16b) bias correction. Note that Figure 16a or 16b is comprised of four subdiagrams to form Panel a or b, respectively, side by side for the purpose of inter-comparison. Apparent ozone recoveries were observed globally through each season by a rate of 1 DU/year, with the most prominent recoveries observed mainly over North America in spring and over East Antarctica in fall by a rate of 4 DU/year (Fig. 16a). In addition, most of the observed ozone layer recoveries were significant at the 90% confidence interval. These results strongly depict the signs of ozone layer recovery at the global scale in the past decade.

Compared to apparent increasing trends derived from the merged TCO time series without bias correction (Fig. 16a), increasing trends were much weaker when derived from the merged time series between bias-corrected OMI and OMPS TCO observations. In addition, most of the increasing trends were not statistically significant at the global scale. Differences between seasonal trends derived from merged time series before and after bias correction (Fig. 17), indicating that trends derived from the merged time series without bias correction apparent overestimated those from bias-corrected time series over most regions throughout the year by an average of 0.531 DU/year in spring (March–April–May), 0.51 DU/year in summer (June–July–August), 0.447 DU/year in fall (September–October–November), and 0.408 DU/year in winter (December–January–February), respectively. Significant

overestimations were observed at mid-to-high latitudes in the NH and slight underestimations over Antarctica. These differences strongly suggest that the bias correction scheme is essential for preparing an accurate long-term TCO record for trend analysis, even with data from highly accurate TCO datasets, especially for the assessment of ozone recovery speed.

## 5. Conclusions

To achieve the goal of creating a long-term coherent TCO record for trend analysis and climate modeling, a modified statistical bias correction method was proposed for removing apparent cross-mission biases between OMPS and OMI TCO observations prior to the data-merging scheme. The proposed bias-correction method is a modified version of the Q-Q adjustment method, with essential modifications made to the bias-estimation algorithms. Compared to the original, the modified method is more adaptive and transferable and can be easily applied to any similar applications. This adaptive characteristic results from the improvements of bias estimation algorithms. In the modified version, biases can be easily quantified for given observations from two control observations through distribution mapping, without dependence on the distribution of raw input observations. By contrast, the original method requires the same length of samples in both raw and control observations, a difficult requirement to satisfy, especially for calibrating long-term satellite observations with limited overlaps.

In these types of statistical bias correction methods, adequate and ample samples are required in control observation time series to guarantee accurate bias estimation, especially for datasets with time-dependent biases, such as TCO observations, because biases are mainly determined from these pair-wise control observations through distribution mapping. Generally, the control observation time series should include observations sampled from a minimum of one complete time period (or one cycle), such as 1-year TCO observations, to remove the seasonal dependent cross-mission biases. Otherwise, biases might not be effectively removed with limited samples in both control observations. In addition, the consistency and quality of each sensor's observations are also critical to the final result, especially for those sensors after years of operation because their quality might be affected due to degradations of sensors. Within this context, accurate instrumental calibrations are indispensable.

Taking advantage of 3-year overlapped observations during 2012–2015, the historical TCO observations from OMI during 2004–2012 were calibrated to the OMPS level at the global scale by using the modified statistical bias correction method. To evaluate the performances of this bias correction method, one time series similarity index termed as overall inconsistency was proposed in this study to quantify the consistency between two time series. Compared to simple statistics, such as the MRD and RMSE, the OI is more versatile and comprehensive in quantifying similarities between time series because it can account for deviations, variances, and correlations, simultaneously. Comparisons of OIs before and after bias correction suggest that the modified bias correction method works effectively in removing observed apparent latitudinal and seasonal dependent cross-mission TCO biases between OMPS and OMI. The consistency was improved significantly after bias correction, with an overall improvement of 90% at the global scale. This prominent improvement could be mainly ascribed to the application of unique control observations at each geographic grid and the seasonal behavior of cross-mission biases. Finally, with bias-corrected OMI TCO observations, a long-term consistent TCO record was created by merging the bias-corrected OMI TCO observations with that of OMPS.

In addition to evaluating consistency improvements before and after bias correction, impacts of cross-mission biases on trend estimations were also investigated. Trends derived from time series without bias correction significantly overestimated those from the bias-corrected time series. Apparent increasing trends were observed from the simply merged TCO time series between OMPS and OMI without bias correction at 38 ground-based stations during 2004–2015, almost twice

those from the original OMI, the bias-corrected time series, and the ground-based measurements. In addition to significant impacts on magnitudes of estimated trends, cross-mission biases also resulted in different phases of trends. Further comparisons of estimated global seasonal TCO trends before and after bias correction suggest that trends derived from the bias corrected time series are more accurate than those without bias correction. Overall, the bias correction scheme is essential for preparing an accurate long-term TCO record for trend analyses, even with data from highly accurate TCO datasets, especially for the assessment of ozone recovery at the global scale.

## Acknowledgements

The authors would like to acknowledge the NASA'S OMPS and OMI science team for their work producing the total column ozone data used in this study. We also thank those scientists preparing the ground-based total column ozone data that are publically available from the World Ozone and UV Data Center (WOUDC). This work was supported by the Science and Technology Commission of Shanghai Municipality (15dz1207805 and 13231203804), Shanghai Municipal Commission of Health and Family Planning (15GWZK0201) and USDA NIFA (2015-34263-24070).

## References

- Ahmed, K. F., Wang, G., Silander, J., Wilson, A. M., Allen, J. M., Horton, R., & Anyah, R. (2013). Statistical downscaling and bias correction of climate model outputs for climate change impact assessment in the U.S. northeast. *Global and Planetary Change*, 100, 320–332. <http://dx.doi.org/10.1016/j.gloplacha.2012.11.003>.
- Amengual, A., Homar, V., Romero, R., Alonso, S., & Ramis, C. (2011). A statistical adjustment of regional climate model outputs to local scales: Application to Platja de Palma, Spain. *Journal of Climate*, 25(3), 939–957. <http://dx.doi.org/10.1175/JCLI-D-10-05024.1>.
- Antón, M., López, M., Vilaplana, J. M., Kroon, M., McPeters, R., Bañón, M., & Serrano, A. (2009). Validation of OMI-TOMS and OMI-DOAS total ozone column using five Brewer spectroradiometers at the Iberian peninsula. *Journal of Geophysical Research*, 114(D14), 1–10. <http://dx.doi.org/10.1029/2009JD012003>.
- Arblaster, J. M., Meehl, G. A., & Karoly, D. J. (2011). Future climate change in the Southern Hemisphere: Competing effects of ozone and greenhouse gases. *Geophysical Research Letters*, 38(2), 1–6. <http://dx.doi.org/10.1029/2010GL045384>.
- Argüeso, D., Evans, J. P., & Fita, L. (2013). Precipitation bias correction of very high resolution regional climate models. *Hydrology and Earth System Sciences*, 17(11), 4379–4388. <http://dx.doi.org/10.5194/hess-17-4379-2013>.
- Bai, K., Chang, N.-B., & Chen, C.-F. (2016). Spectral information adaptation and synthesis scheme for merging cross-mission ocean color reflectance observations from MODIS and VIIRS. *IEEE Transactions on Geoscience and Remote Sensing*, 54(1), 311–329. <http://dx.doi.org/10.1109/TGRS.2015.2456906>.
- Bai, K., Liu, C., Shi, R., & Gao, W. (2015). Comparison of Suomi-NPP OMPS total column ozone with Brewer and Dobson spectrophotometers measurements. *Frontiers of Earth Science*, 9(3), 369–380. <http://dx.doi.org/10.1007/s11707-014-0480-5>.
- Bak, J., Liu, X., Kim, J. H., Chance, K., Haffner, D. P., & Systems, S. (2015). Validation of OMI total ozone retrievals from the SAO ozone profile algorithm and three operational algorithms with Brewer measurements. *Atmospheric Chemistry and Physics*, 15(2), 667–683. <http://dx.doi.org/10.5194/acp-15-667-2015>.
- Balis, D., Kroon, M., Koukoulis, M. E., Brinksma, E. J., Labow, G., Veefkind, J. P., & McPeters, R. D. (2007). Validation of Ozone Monitoring Instrument total ozone column measurements using Brewer and Dobson spectrophotometer ground-based observations. *Journal of Geophysical Research*, 112(D24), D24S46. <http://dx.doi.org/10.1029/2007JD008796>.
- Barnes, B. B., & Hu, C. (2015). Cross-sensor continuity of satellite-derived water clarity in the Gulf of Mexico: Insights into temporal aliasing and implications for long-term water clarity assessment. *IEEE Transactions on Geoscience and Remote Sensing*, 53(4), 1761–1772. <http://dx.doi.org/10.1109/TGRS.2014.2348713>.
- Barnes, E. A., Barnes, N. W., & Polvani, L. M. (2014). Delayed southern hemisphere climate change induced by stratospheric ozone recovery, as projected by the CMIP5 models. *Journal of Climate*, 27(2), 852–867. <http://dx.doi.org/10.1175/JCLI-D-13-00246.1>.
- Basher, R. E. (1982). *Review of the Dobson spectrophotometer and its accuracy. Global ozone research and monitoring project-report 13* (Geneva, Switzerland).
- Bass, A. M., & Paur, R. J. (1985). The ultraviolet cross section of ozone. I. the measurements. *Proceedings of the quadrennial ozone symposium* (pp. 606–616). [http://dx.doi.org/10.1007/978-94-009-5313-0\\_120](http://dx.doi.org/10.1007/978-94-009-5313-0_120).
- Bhartia, P. K., & Wellemeyer, C. W. (2002). *TOMS-V8 total O3 algorithm. OMI algorithm theoretical basis document, volume II, OMI ozone products* Washington, DC: NASA-OMI.
- Bhartia, P. K., McPeters, R. D., Flynn, L. E., Taylor, S., Kramarova, N. A., Frith, S., ... DeLand, M. (2013). Solar Backscatter UV (SBUV) total ozone and profile algorithm. *Atmospheric Measurement Techniques*, 6(10), 2533–2548. <http://dx.doi.org/10.5194/amt-6-2533-2013>.
- Bordoy, R., & Burlando, P. (2013). Bias correction of regional climate model simulations in a region of complex orography. *Journal of Applied Meteorology and Climatology*, 52(1), 82–101. <http://dx.doi.org/10.1175/JAMC-D-11-0149.1>.

- Brewer, A. W. (1973). A replacement for the Dobson spectrophotometer? *Pure and Applied Geophysics*, 106–108(1), 919–927. <http://dx.doi.org/10.1007/BF00881042>.
- D'Alimonte, D., Zibordi, G., & Melin, F. (2008). A statistical method for generating cross-mission consistent normalized water-leaving radiances. *IEEE Transactions on Geoscience and Remote Sensing*, 46(12), 4075–4093. <http://dx.doi.org/10.1109/TGRS.2008.2001819>.
- Delle Monache, L., Nipen, T., Deng, X., Zhou, Y., & Stull, R. (2006). Ozone ensemble forecasts: 2. A Kalman filter predictor bias correction. *Journal of Geophysical Research - Atmospheres*, 111(5), 1–15. <http://dx.doi.org/10.1029/2005JD006311>.
- Ding, Q., Steig, E. J., Battisti, D. S., & Küttel, M. (2011). Winter warming in West Antarctica caused by central tropical Pacific warming. *Nature Geoscience*, 4(6), 398–403. <http://dx.doi.org/10.1038/ngeo1129>.
- Dobson, G. M. B. (1968). Forty years' research on atmospheric ozone at Oxford: A history. *Applied Optics*, 7(3), 387–405. <http://dx.doi.org/10.1364/AO.7.000387>.
- Dragani, R. (2011). On the quality of the ERA-interim ozone reanalyses: Comparisons with satellite data. *Quarterly Journal of the Royal Meteorological Society*, 137(658), 1312–1326. <http://dx.doi.org/10.1002/qj.821>.
- Feldstein, S. B. (2011). Subtropical rainfall and the Antarctic ozone hole. *Science*, 332(6032), 925–926. <http://dx.doi.org/10.1126/science.1206834>.
- Flynn, L., Hornstein, J., & Hilsenrath, E. (2004). The ozone mapping and profiler suite (OMPS). *Proceedings of IEEE International Geoscience and Remote Sensing Symposium*, 1. (pp. 152–155). <http://dx.doi.org/10.1109/IGARSS.2004.1368968>.
- Flynn, L., Long, C., Wu, X., Evans, R., Beck, C. T., Petropavlovskikh, I., ... Sefor, C. (2014). Performance of the ozone mapping and profiler suite (OMPS) products. *Journal of Geophysical Research - Atmospheres*, 119(10), 6181–6195. <http://dx.doi.org/10.1002/2013JD020467>.
- Frith, S. M., Kramarova, N. A., Stolarski, R. S., McPeters, R. D., Bhartia, P. K., & Labow, G. J. (2014). Recent changes in total column ozone based on the SBUV Version 8.6 merged ozone data set. *Journal of Geophysical Research - Atmospheres*, 119(16), 9735–9751. <http://dx.doi.org/10.1002/2014JD021889>.
- Fyfe, J. C., Gillett, N. P., & Marshall, G. J. (2012). Human influence on extratropical Southern Hemisphere summer precipitation. *Geophysical Research Letters*, 39(23), L23711. <http://dx.doi.org/10.1029/2012GL054199>.
- WMO (2003). Global Ozone Research and Monitoring Project. Scientific Assessment of Ozone Depletion: 2002. Report No. 47, World Meteorological Organization, Geneva.
- Gerelchuluun, B., & Ahn, J. B. (2014). Air temperature distribution over Mongolia using digital downscaling and statistical correction. *International Journal of Climatology*, 34(7), 2464–2476. <http://dx.doi.org/10.1002/joc.3853>.
- Gillett, N. P., Fyfe, J. C., & Parker, D. E. (2013). Attribution of observed sea level pressure trends to greenhouse gas, aerosol, and ozone changes. *Geophysical Research Letters*, 40(10), 2302–2306. <http://dx.doi.org/10.1002/grl.50500>.
- Gonzalez, P. L. M., Polvani, L. M., Seager, R., & Correa, G. J. P. (2013). Stratospheric ozone depletion: A key driver of recent precipitation trends in south eastern South America. *Climate Dynamics*, 42(7–8), 1775–1792. <http://dx.doi.org/10.1007/s00382-013-1777-x>.
- Gregg, W. W., & Casey, N. W. (2010). Improving the consistency of ocean color data: A step toward climate data records. *Geophysical Research Letters*, 37(4), L04605. <http://dx.doi.org/10.1029/2009GL041893>.
- Haerter, J. O., Hagemann, S., Moseley, C., & Piani, C. (2011). Climate model bias correction and the role of timescales. *Hydrology and Earth System Sciences*, 15(3), 1065–1079. <http://dx.doi.org/10.5194/hess-15-1065-2011>.
- Hagemann, S., Chen, C., Haerter, J. O., Heinke, J., Gerten, D., & Piani, C. (2011). Impact of a statistical bias correction on the projected hydrological changes obtained from three GCMs and two hydrology models. *Journal of Hydrometeorology*, 12(4), 556–578. <http://dx.doi.org/10.1175/2011JHM1336.1>.
- Hoyer, J. L., Le Borgne, P., & Eastwood, S. (2013). A bias correction method for Arctic satellite sea surface temperature observations. *Remote Sensing of Environment*, 146, 201–213. <http://dx.doi.org/10.1016/j.rse.2013.04.020>.
- Jöckel, P., Tost, H., Pozzer, A., Brühl, C., Buchholz, J., Ganzeveld, L., ... Lelieveld, J. (2006). The atmospheric chemistry general circulation model ECHAM5/MESy1: Consistent simulation of ozone from the surface to the mesosphere. *Atmospheric Chemistry and Physics*, 6(4), 5067–5114. <http://dx.doi.org/10.5194/acp-6-5067-2006>.
- Kang, S. M., Polvani, L. M., Fyfe, J. C., & Sigmond, M. (2011). Impact of polar ozone depletion on subtropical precipitation. *Science*, 332(6032), 951–954. <http://dx.doi.org/10.1126/science.1202131>.
- Kramarova, N. A., Nash, E. R., Newman, P. A., Bhartia, P. K., McPeters, R. D., Rault, D. F., ... Labow, G. J. (2014). Measuring the Antarctic ozone hole with the new ozone mapping and profiler suite (OMPS). *Atmospheric Chemistry and Physics*, 14(5), 2353–2361. <http://dx.doi.org/10.5194/acp-14-2353-2014>.
- Kuttippurath, J., Lefèvre, F., Pommereau, J.-P., Roscoe, H. K., Goutail, F., Pazmiño, A., & Shanklin, J. D. (2013). Antarctic ozone loss in 1979–2010: First sign of ozone recovery. *Atmospheric Chemistry and Physics*, 13(3), 1625–1635. <http://dx.doi.org/10.5194/acp-13-1625-2013>.
- Lafon, T., Dadson, S., Buys, G., & Prudhomme, C. (2013). Bias correction of daily precipitation simulated by a regional climate model: A comparison of methods. *International Journal of Climatology*, 33(6), 1367–1381. <http://dx.doi.org/10.1002/joc.3518>.
- Lerot, C., Van Roozendaal, M., Spurr, R., Loyola, D., Coldewey-Egbers, M., Kochenova, S., ... Zehner, C. (2014). Homogenized total ozone data records from the European sensors GOME/ERS-2, SCIAMACHY/Envisat, and GOME-2/MetOp-A. *Journal of Geophysical Research - Atmospheres*, 119(3), 1639–1662. <http://dx.doi.org/10.1002/2013JD020831>.
- Levelt, P. F., van den Oord, G. H. J., Dobber, M. R., Malkki, A., Stammes, P., Lundell, J. O. V., & Saari, H. (2006). The ozone monitoring instrument. *IEEE Transactions on Geoscience and Remote Sensing*, 44(5), 1093–1101. <http://dx.doi.org/10.1109/TGRS.2006.872333>.
- Lhermitte, S., Verbesselt, J., Verstraeten, W. W., & Coppin, P. (2011). A comparison of time series similarity measures for classification and change detection of ecosystem dynamics. *Remote Sensing of Environment*, 115(12), 3129–3152. <http://dx.doi.org/10.1016/j.rse.2011.06.020>.
- Li, H., Sheffield, J., & Wood, E. F. (2010). Bias correction of monthly precipitation and temperature fields from intergovernmental panel on climate change AR4 models using equidistant quantile matching. *Journal of Geophysical Research - Atmospheres*, 115(10). <http://dx.doi.org/10.1029/2009JD012882>.
- Loyola, D. G., & Coldewey-Egbers, M. (2012). Multi-sensor data merging with stacked neural networks for the creation of satellite long-term climate data records. *EURASIP Journal on Advances in Signal Processing*, 2012(1), 91. <http://dx.doi.org/10.1186/1687-6180-2012-91>.
- Mahalanobis, P. C. (1936). On the generalised distance in statistics. *Proceedings of the National Institute of Sciences of India*, 2(1), 49–55.
- Malicet, J., Daumont, D., Charbonnier, J., Parisse, C., Chakir, A., & Brion, J. (1995). Ozone UV spectroscopy. II. Absorption cross-sections and temperature dependence. *Journal of Atmospheric Chemistry*, 21(3), 263–273. <http://dx.doi.org/10.1007/BF00696758>.
- Manatsa, D., Morioka, Y., Behera, S. K., Yamagata, T., & Matarira, C. H. (2013). Link between Antarctic ozone depletion and summer warming over southern Africa. *Nature Geoscience*, 6(11), 934–939. <http://dx.doi.org/10.1038/ngeo1968>.
- McPeters, R. D., Bhartia, P. K., Haffner, D., Labow, G. J., & Flynn, L. (2013). The version 8.6 SBUV ozone data record: An overview. *Journal of Geophysical Research - Atmospheres*, 118(14), 8032–8039. <http://dx.doi.org/10.1002/jgrd.50597>.
- Osca, J., Romero, R., & Alonso, S. (2013). Precipitation projections for Spain by means of a weather typing statistical method. *Global and Planetary Change*, 109, 46–63. <http://dx.doi.org/10.1016/j.gloplacha.2013.08.001>.
- Perlwitz, J. (2011). Atmospheric science: Tug of war on the jet stream. *Nature Climate Change*, 1(1), 29–31. <http://dx.doi.org/10.1038/nclimate1065>.
- Perlwitz, J., Pawson, S., Fogt, R. L., Nielsen, J. E., & Neff, W. D. (2008). Impact of stratospheric ozone hole recovery on Antarctic climate. *Geophysical Research Letters*, 35(8), 1–5. <http://dx.doi.org/10.1029/2008GL033317>.
- Piani, C., Haerter, J. O., & Coppola, E. (2010). Statistical bias correction for daily precipitation in regional climate models over Europe. *Theoretical and Applied Climatology*, 99(1–2), 187–192. <http://dx.doi.org/10.1007/s00704-009-0134-9>.
- Piani, C., Weedon, G. P., Best, M., Gomes, S. M., Viterbo, P., Hagemann, S., & Haerter, J. O. (2010). Statistical bias correction of global simulated daily precipitation and temperature for the application of hydrological models. *Journal of Hydrology*, 395(3–4), 199–215. <http://dx.doi.org/10.1016/j.jhydrol.2010.10.024>.
- Previdi, M., & Polvani, L. M. (2014). Climate system response to stratospheric ozone depletion and recovery. *Quarterly Journal of the Royal Meteorological Society*, 140(685), 2401–2419. <http://dx.doi.org/10.1002/qj.2330>.
- Reason, C. J. C. (2005). Links between the Antarctic oscillation and winter rainfall over western South Africa. *Geophysical Research Letters*, 32(7), L07705. <http://dx.doi.org/10.1029/2005GL022419>.
- Sefor, C. J., Jaross, G., Kowitz, M., Haken, M., Li, J., & Flynn, L. E. (2014). Postlaunch performance of the Suomi national polar-orbiting partnership ozone mapping and profiler suite (OMPS) nadir sensors. *Journal of Geophysical Research - Atmospheres*, 119(7), 4413–4428. <http://dx.doi.org/10.1002/2013JD020472>.
- Sicardi, V., Ortiz, J., Rincón, A., Jorba, O., Pay, M. T., Gassó, S., & Baldasano, J. M. (2012). Assessment of Kalman filter bias-adjustment technique to improve the simulation of ground-level ozone over Spain. *Science of the Total Environment*, 416, 329–342. <http://dx.doi.org/10.1016/j.scitotenv.2011.11.050>.
- Son, S.-W., Tandon, N. F., Polvani, L. M., & Waugh, D. W. (2009). Ozone hole and Southern Hemisphere climate change. *Geophysical Research Letters*, 36(15), L15705. <http://dx.doi.org/10.1029/2009GL038671>.
- Teutschbein, C., & Seibert, J. (2012). Bias correction of regional climate model simulations for hydrological climate-change impact studies: Review and evaluation of different methods. *Journal of Hydrology*, 456–457, 12–29. <http://dx.doi.org/10.1016/j.jhydrol.2012.05.052>.
- Teutschbein, C., & Seibert, J. (2013). Is bias correction of regional climate model (RCM) simulations possible for non-stationary conditions. *Hydrology and Earth System Sciences*, 17(12), 5061–5077. <http://dx.doi.org/10.5194/hess-17-5061-2013>.
- Thompson, D. W. J., Solomon, S., Kushner, P. J., England, M. H., Grise, K. M., & Karoly, D. J. (2011). Signatures of the Antarctic ozone hole in Southern Hemisphere surface climate change. *Nature Geoscience*, 4(11), 741–749. <http://dx.doi.org/10.1038/ngeo1296>.
- Van Der, A. J., R., Allaart, M. A. F., & Eskes, H. J. (2010). Multi sensor reanalysis of total ozone. *Atmospheric Chemistry and Physics*, 10(22), 11277–11294. <http://dx.doi.org/10.5194/acp-10-11277-2010>.
- Van der, A., J., R., Allaart, M. A. F., & Eskes, H. J. (2015). Extended and refined multi sensor reanalysis of total ozone for the period 1970–2012. *Atmospheric Measurement Techniques Discussions*, 8(3), 3283–3319. <http://dx.doi.org/10.5194/amtd-8-3283-2015>.
- Van Roozendaal, M., Peeters, P., Roscoe, H. K., De Backer, H., Jones, A. E., Bartlett, L., ... Simon, P. C. (1998). Validation of ground-based visible measurements of total ozone by comparison with Dobson and Brewer spectrophotometers. *Journal of Atmospheric Chemistry*, 29(1), 55–83. <http://dx.doi.org/10.1023/A:1005815902581>.
- Veefkind, J. P., De Haan, J. F., Brinksma, E. J., Kroon, M., & Levelt, P. F. (2006). Total ozone from the ozone monitoring instrument (OMI) using the DOAS technique. *IEEE Transactions on Geoscience and Remote Sensing*, 44(5), 1239–1244. <http://dx.doi.org/10.1109/TGRS.2006.871204>.
- Vila, D. A., de Goncalves, L. G. G., Toll, D. L., & Rozante, J. R. (2009). Statistical evaluation of combined daily gauge observations and rainfall satellite estimates over continental South America. *Journal of Hydrometeorology*, 10(2), 533–543. <http://dx.doi.org/10.1175/2008JHM1048.1>.
- Wu, X., Liu, Q., Zeng, J., Grotenhuis, M., Qian, H., Caponi, M., ... Li, W. -H. (2014). Evaluation of the sensor data record from the nadir instruments of the ozone mapping profiler suite (OMPS). *Journal of Geophysical Research - Atmospheres*, 119(10), 6170–6180. <http://dx.doi.org/10.1002/2013JD020484>.